Università degli Studi di Udine
Dottorato di Ricerca in
Tecnologie Chimiche ed Energetiche
XXIV Ciclo

ANALYSIS AND CHARACTERIZATION OF HEAT AND MASS TRANSFER IN ROTARY EXCHANGERS

Dott. Ing. Olivo PASCOLI

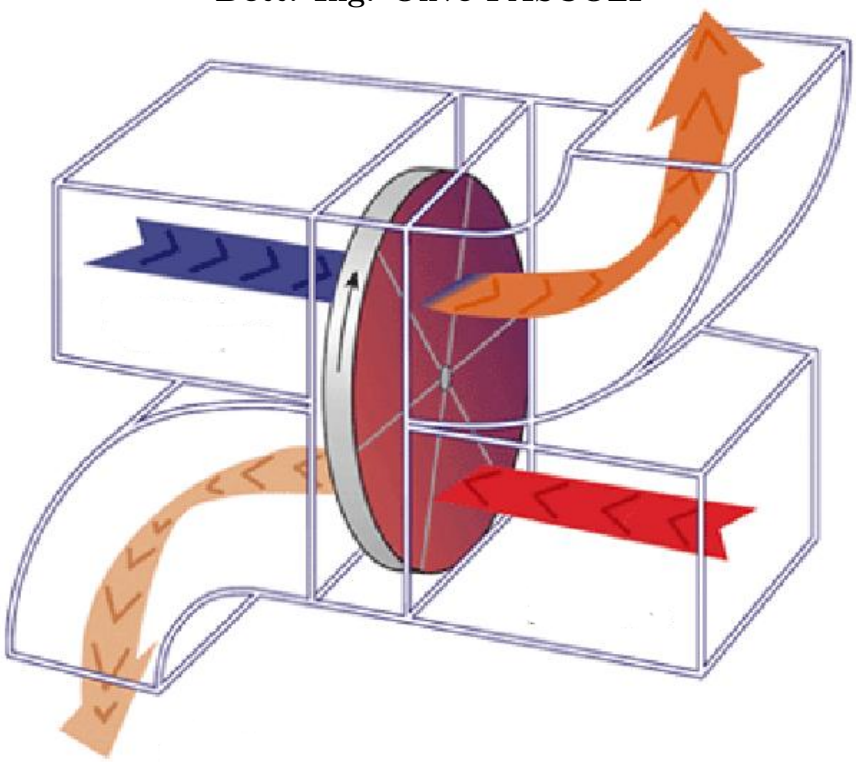

COMMISSIONE

Dr. Prof. Martino MARINI	Revisore
Dr. Prof. Gian Luca MORINI	Revisore
Dr. Prof. Enrico NOBILE	Commissario
Dr. Prof. Pietro DE PALMA	Commissario
Dr. Prof. Tommaso ASTARITA	Commissario
Dr. Prof. Giulio CROCE	Supervisore
Dr. Prof. Alfredo SOLDATI	Coordinatore del Dottorato

Author's Web Page: www.diegm.uniud.it

Author's e-mail: olivo.pascoli@uniud.com

Author's address:

Dipartimento di Ingegneria Elettrica
Gestionale e Meccanica
Università degli Studi di Udine
Via delle Scienze, 106
33100 Udine – Italia
tel. +39 0432 558031
fax. +39 0432 558251
web: http://www.diegm.uniud.it

UDINE printed in March 2012

To Silvia,
for her care, support and love in all these years.
Thank you!

Abstract

Integration of the energy recovery system with a traditional HVAC system has gained recent attention because of the potential for energy savings. A popular choice for the energy recovery system include a rotary air-to-air energy wheel with a porous matrix as the heat and moisture transfer medium. The wheel is in general symmetrical and balanced, operating with counter-flow pattern. The primary goal of this research is to develop a mathematical and numerical model to predict the effectiveness of such energy wheel.

Two different models were developed for rotary exchangers: a sensible model and a enthalpy model. The sensible model describes the pure heat transfer phenomenon in a rotary wheel with a non -desiccant porous matrix. This require the introduction of two coupled energy conservation equations for the solid and the fluid. The enthalpy model describes the combined heat and mass transfer process in a rotary wheel coated with a desiccant porous media, allowing for adsorption and desorption. In this case, the process can be mathematically represented by two energy conservation equations and two mass conservation equations, plus the proper closure relationships describing saturation properties of moist air and the dessiccant behaviour.

The study evaluated the effect of the main wheel design parameters, including rotational speed, number of transfer units, heat capacity and desiccant material. A wide range of operating parameters (volume flow rate, inlet air temperatures and humidity ratios) were considered and the numerical results are compared with experimental results. Experimental data of effectiveness obtained from commercial unit are found to be consistent with the numerical results.

Acknowledgments

A heartfelt thanks to the staff of the Department DIEGM of University of Udine who have worked directly but also indirectly to the success of this work.
In particular I would like to express my sincere gratitude and appreciation to my adviser Professor G.Croce. Thank you for providing ideas, guidance, assistance and editing throughout this research. I would like to extend my sincere appreciation to Professor G. Comini for supporting and encouraging me in this work.
Lastly but not the least, I would like to acknowledge the help of Geo.Coil srl (Italy) for letting me use their experimental and technological facility about the rotary exchangers.

Contents

List of Figures

List of Tables

Preface

Imagination is more important than knowledge. For knowledge is limited to all we now know and understand, while imagination embraces the entire world, and all there ever will be to know and understand.

A.Einstein

1 Introduction

1.1 Background

Indoor air quality (IAQ) which describes the nature of air inside the building is an important parameter, since people often spend up 85-90% of their time indoors. The American Society of Heating, Refrigerating and Air-Conditioning Engineers (ASHRAE) defines the indoor air quality as "an acceptable comfort level to 80% of the people exposed to it". In order to maintain an acceptable IAQ in a closed building a proper ventilation is required, either simply through open windows or using mechanical ventilation. The latter solutions allows a much stricter control on the mass flow rates, and make it easier to introduce heat recovery systems to the reduce the thermal load of HVAC systems. Furthermore, for energy saving purposes, modern buildings are typically insulated as much as possible from the outside environment. Thus, mechanical ventilation is obviously the most appropriate way to provide the optimal (in term of energy balances) quantity of fresh outdoor air into the sealed house and discharge the exhausted indoor air.

Mechanical ventilation in buildings became common in the fifties, although early application dates backed to the early 1900s, and quantitative constraint have been imposed to these ventilation systems since a few decades ago, in order to preserve occupants thermal and hygrometric comfort, as well as energy efficiency: in 1973, the American Society of Heating, Refrigeration and Air Conditioning Engineers (ASHRAE) approved the first version of Standard 62, which was titled Standard 62-73, "Standard for Natural and Mechanical Ventilation" [1]. This Standard required a minimum of 10 cfm per person of outside air, but recommended outside air ventilation rates in the 15 to 25 cfm per person range. In 1981, ASHRAE Standard 62-73 was revised as Standard 62-81 and renamed "Ventilation for Acceptable Indoor Air Quality" [2]. ASHRAE Standard 62-1989 specified "minimum ventilation rates and indoor air quality that will be acceptable to human occupants and is intended to minimize the potential for adverse health effects" [3]. Since then, the Standard 62−1989 was under continuous maintenance, which allowed ASHRAE to update the standard on an ongoing basis through the addition of addenda and new sections. A number of additional addenda are under development to convert the Standard 62 into a "code-intended language" [4].
Controlling humidity inside the house is essential in order to achieve high indoor environmental quality. Microbial growth and building material tear are the results of humidity

in excess of 60%, while human discomfort, ranging from dry skin to respiratory irritation, results from dry indoor air below 30% [5]. For these reasons, ASHRAE has developed a thermal comfort Standard 55−1992 [ll], which identities temperature and humidity conditions (30-60%) that will satisfy 80% or more of building occupants.

In the 2002 ASHRAE equipment handbook [6], the most popular six types of air-to-air heat exchange devices are presented. Some of them are pure sensible heat exchangers, others may serve as total energy exchangers (sensible and latent) as well. The rotary air−to−air energy wheel is one of these flexible devices which can be designed as either sensible or total. A total energy wheel (sensible and latent) may provide an increased comfort while reducing HVAC system capital and operating costs. In terms of energy recovery, the heat recovery of a total energy device may be up to three times that of a simpler sensible heat recovery one. A survey of typical effectiveness and pressure drop data for different recovery devices shows that the energy wheel has the highest effectiveness and least pressure drop at any face velocity, making it the most appropriate choice for energy recovery in comfort ventilation [6].

1.2 Objects of this work

The central goal of this research is to develop an understanding of the heat and mass transfer processes which occur in a porous matrix rotary energy wheel, with the aim of building a numerical model flexible enough to be (in perspective) integrated with complex CFD modeling.

A review of the literature reveals that considerable information is available regarding energy wheels: in most cases experimental data are compared with either empirical correlations ([7],[8],[9],[10],[11],[12]) or some kind of simplified numerical model ([13] , [14], [15],[16],[17],[18],[19], [20],[21],[22],[23] , [24], [25]). The numerical models investigated the flow inside the channel with heat and mass trasfer.

The energy wheel selected for this research is a rotary wheel acting as a heat and moisture exchange medium operating in counter-flow arrangement. The objectives of this research are to:

1. Develop a numerical model to predict the performance of a sensible heat wheel without condensation (sensible model).

2. Develop a numerical model to predict the performance of a desiccant wheel for enthalpy recovery application (enthalpy model).

3. Compare the models with existing effectiveness correlations and with some experimental data.

The main objective of this research is to provide the engineering community with a reliable enthalpy wheel model readily applicable to design and/or analysis of enthalpy wheel applications. It is expected that such model, based on several theoretical aspitions, should be much more flexible than current correlations, offering more freedom to

the designe. The two enthalpy wheel materials most widely used in the industry today are considered: silica gel and molecular sieve loaded on an aluminium substrate.

ln the present thesis, geometrical properties, coordinates, and dimensionless parameters for the air-to-air rotary energy wheel under investigation will be first established, in order to have a basis for the models that will be developed (heat transfer model and enthalpy model). A mathematical model for a porous media based energy wheel will be developed based on the physical principles of the operation of the energy wheels. The model is 3D dimensional and transient in time (t). The thermodynamic relationships will be discussed for each model since the models can have different thermodynamic relationships. Enthalpy and temperature formulation will be developed for each model. A complete dimensionless representation for each model will be accomplished. The initial and boundary conditions will be defined for the supply and exhaust side. In this phase of the research we will establish the governing equations of the models. In the second step, we choose the numerical method and computer codes structures. All the governing equations of the energy wheel will be solved numerically by finite element analysis software because the equations are strongly coupled, iterations are necessary to get converged values for each time steps. The numerical formulation model was implemented in the COMSOL sotware. The codes are designed to simulate the wheel from an initial condition until steady state (in an Eulerian sense) is reached. The heat transfer numerical model will be used to examine the effectiveness of the wheel under summer and winter conditions. Effects of the rotational speed ω , the global number of transfer unit NTU_o, the matrix exchanger heat capacity-ratio C_r^*, porosity ϕ , volume flow rate $\dot{V}$ will be studied and compared with theoretical results. The temperature profiles of the wheel will also be investigated to study the behaviour of the wheel. As the final modelling study, a numerical code will be developed for the enthalpy wheel model. The sorption isotherm for the matrix material will be modelled. Results will be compared with experimental and theoretical results.

2

Operation principle of rotary exchangers

2.1 Description of rotary heat exchangers

Rotary regenerators and recuperators are widely used in a broad range of industrial applications, from low temperature air conditioning systems to large power plant energy recovery systems. All of them, however, can be schematized as in Fig. 2.1. An air-permeable rotating disk or wheel is located in a duct-work system consisting of a pair of rectangular ducts. The upper half of the disk is fed by hot air moving from right to left through the upper duct, while the lower half of the disk is fed by cooler air flowing from left to right through the other duct. Since the wheel is rotating, it is periodically exposed to both cold and hot streams: during one half of the rotation the wheel solid matrix is heated by the hot stream, and transfers this heat flux to the cold flow during the second half of the rotation.

Usually, the disk consists of a large number of parallel flow passages in the axial direction. In most cases, the wall of the flow passages are obtained stacking sinusoidal or wavy metallic (aluminum) bands (Fig. 2.2 and 2.3), but plastics or ceramic have also been used for limited service.

While the energy and economical benefits of enthalpy wheels in HVAC applications has been known to the engineering community for some time, there have not been practical, easy to use, and reliable enthalpy wheel analytical models because of their complex characteristics of combined heat and mass transfer. The performances of the rotary exchangers are strongly dependent on the types and configurations of energy wheel. Exchange media of the energy wheel con be designed to recovery sensible heat or total energy (sensible and latent). The manufacturers' performance data produced in accordance with ANSI/ARI Standard 1060/2001 are usually used for peak design.

2.2 Classification of rotary exchangers

Three types of heat and mass rotary energy wheels are used in air conditioning system [26]. They are namely the sensible heat wheel, the dehumidifier wheel, and the enthalpy

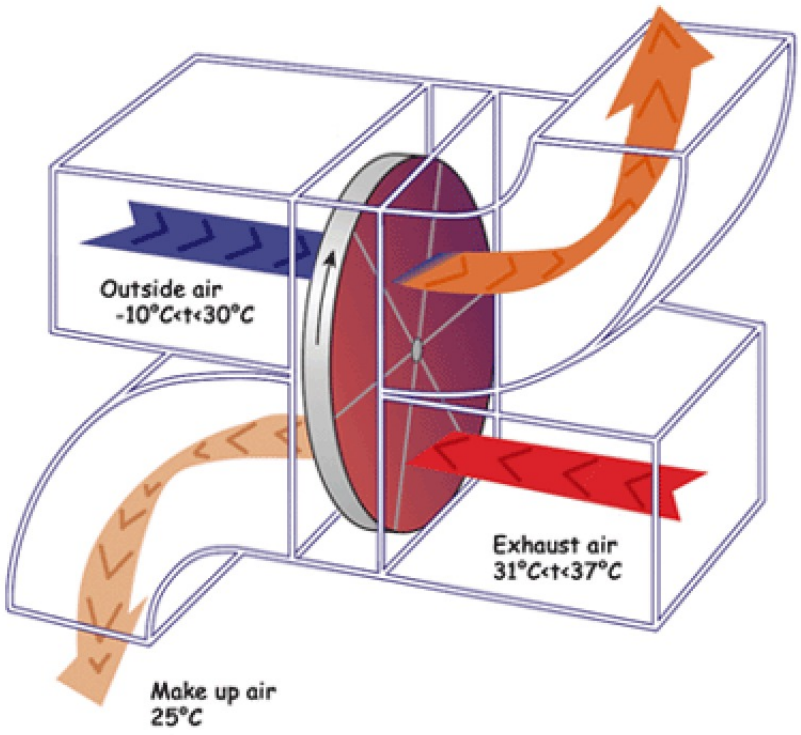

Figure 2.1: Example of installed rotary regenerator

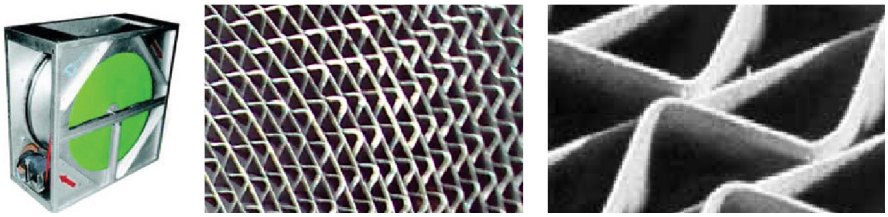

Figure 2.2: Example of porous matrix

(sensible and latent heat) wheel. For the same inlet air temperatures and humidities, each wheel operates with the same principles; however, different outlet temperatures and humidities are expected due to the capability of the wheel to transfer either heat or moisture or both. The performance characteristics of the wheel are largely determined by the physical properties of the porous matrix. Sensible heat wheels require a non−sorbing matrix with large thermal capacity since only heating and cooling of air streams is de-

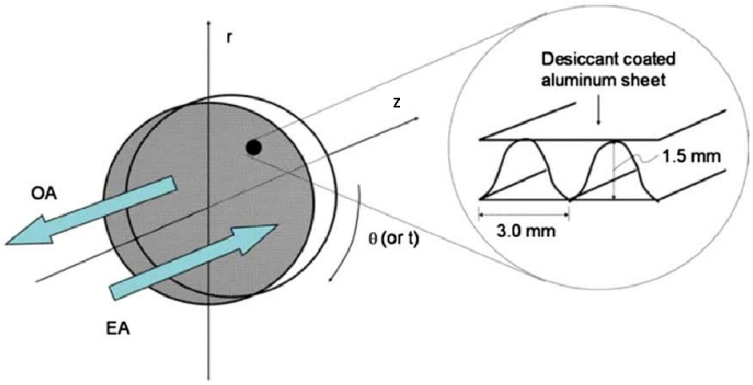

Figure 2.3: Detailed structure of rotary exchanger

sired. Maximum moisture transfer is important in dehumidifier wheels, so they utilize a adsorbent matrix with large moisture capacity but small thermal capacity. Enthalpy wheels employ a absorbent matrix with large thermal and moisture capacity, since both heat and mass transfer are desired.
Sensible heat wheels are used for heat recovery from exhaust air in air conditioning, but total heat wheels give great total heat recovery in hot humid and cold areas.
Dehumidifier wheels are used when low humidities are required in air conditioning.

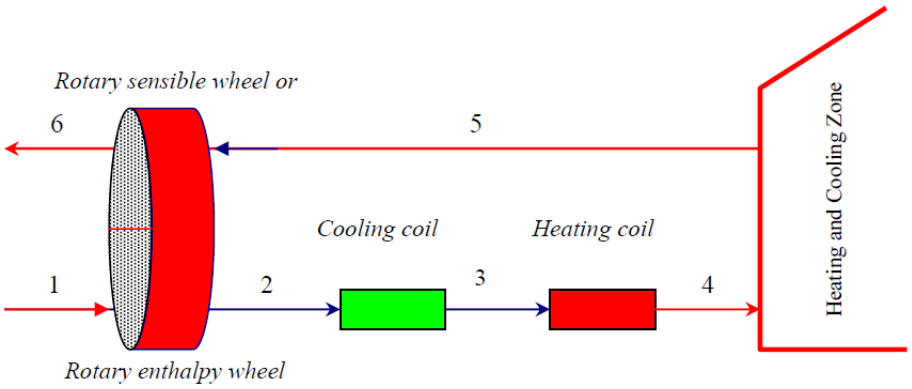

Figure 2.4: Space conditioning system with energy recovery unit

To discuss the basic performance differences between the sensible heat exchanger and the enthalpy exchanger, a typical application of these two exchangers in a space-

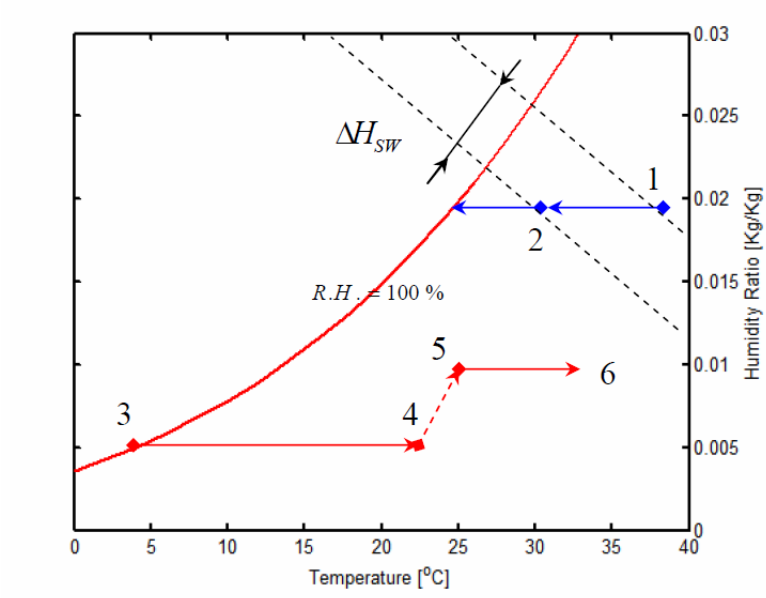

Figure 2.5: Using a sensible wheel (SW) in the air cooling mode (summer)

conditioning system is depicted in Fig 2.4 . In summer, state−1 represents hot outdoor air which will be cooled by colder exhaust air state−5. In winter, state-1 represents cold outdoor air which will be preheated by warmer exhaust air state-5. To demonstrate the performance of both sensible and enthalpy wheels in the air-conditioning application, the summer (cooling mode) season scenario will be used. In the airconditioning application, plotting the inlet and outlet fluid state of such system on a psychometric chart is a convenient way to investigate its performance. In the case of sensible wheel (Fig 2.5), the humidity ratios of the two air streams remain constant throughout the process since only heat transfer is possible. In the case of enthalpy wheel (Fig 2.6), the humidity ratios change due to the combined heat and mass transfer process. Because of this, the outlet states lies on a straight line connecting the two inlet states. From Fig.2.5 and 2.6it is obvious that the amount of energy recovered by the enthalpy exchanger (ΔH_{SW}) is considerably greater than the amount of energy recovered by a sensible heat exchanger(ΔH_{EW}).

Applications of energy wheels in the desiccant cooling cycles have received great attention recently. Fig 2.7 shows the schematic chart of the ventilation solid desiccant air cooling cycle with two regenerative components. The rotary sensible heat wheel consists of a non−hygroscopic matrix whereas the rotary enthalpy contains a solid desiccant material (hygroscopic). ln the ventilation cycle, the desiccant dehumidifier wheel takes the fresh outside air (state−1) and humidities it (state−2). During the sorption process

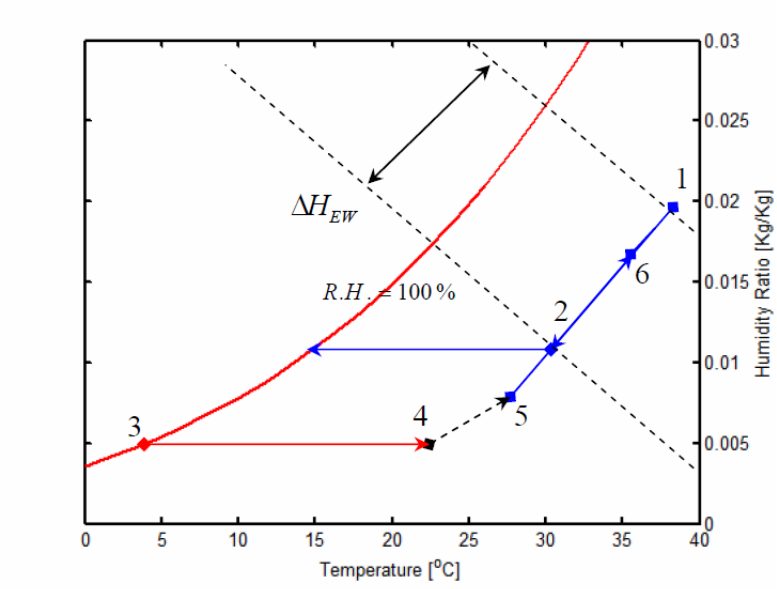

Figure 2.6: Using a enthalpy wheel (EW) in the air cooling mode (summer)

(water vapor adsorbed by the desiccant material), the temperature of the air also rises due to the heat of sorption release. Sensible heat wheel is used to cool the air stream at (state− 2) without changing its humidity ratio to (state− 3) using evaporatively cooled exhaust air (state− 6). The desired level of the temperature and humidity of supply air stream is not accomplished so the supply air stream is evaporatively cooled (state− 4) and passed to the space to be conditioned (state− 5). The sensible heat wheel picks up the heat from hot air stream (state− 2) and releases it to the exhaust cold air stream (state− 7). If the temperature at (state−7) is not enough to regenerate the matrix of the dehumidifier wheel, additional heat source is needed to reach the required regeneration temperature (state− 8). Finally, the desiccant matrix is regenerated (moisture removed) by the hot air stream (state− 9).

Several conditioning systems that use multiple rotary regenerators have been studied and developed: placing two different recovery wheel (one only sensible and one only dehumidifier) we can determine exactly the need but these systems have at least double pressure load losses and double cost. This fact makes such systems economically viable only in certain conditions and the enthapy wheel a good solution.
The present model could be easily applied to multiple system, just by stacking wheels in series.

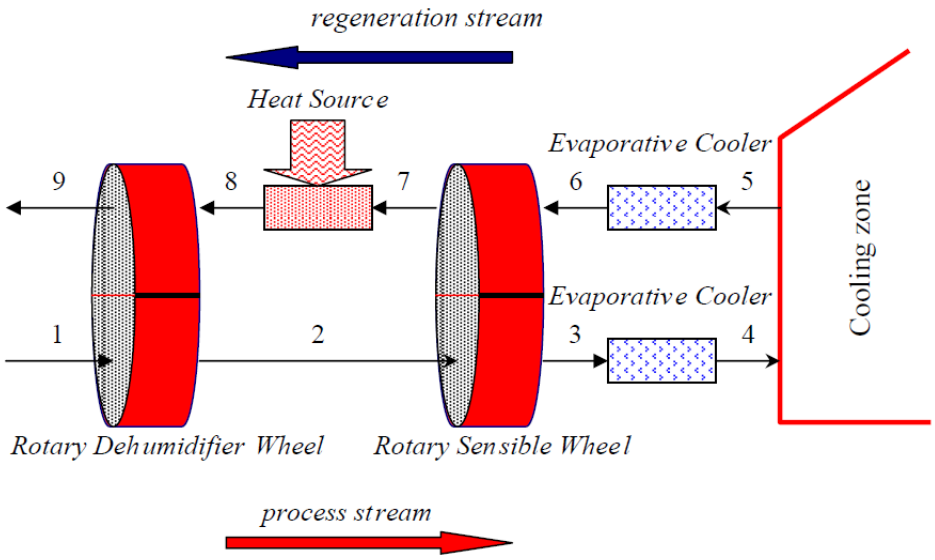

Figure 2.7: Schematic chart ot the ventilation cycle two wheel air conditioning system

2.3 State of the art

2.3.1 Sensible wheel

A rotary air-to-air sensible wheel with non-desiccant matrix usually transfers only sensible heat from the hot to the cold air stream through the transfer media (matrix). On a psychometric chart, the resulting outlet states are both on horizontal lines with inlet states which represent the corresponding inlet humidity ratios. Therefore, the sensible wheel is used to heat or cool the air stream without changing its humidity ratio. In the earlier stages of the development of modelling sensible heat regenerators the lack of a closed-form analytical solution limited the advancements in the industry of regenerators. The available solutions were either an analytical solution to a over simplified problem or graphical solutions using complicated graphical techniques. Therefore, investigation a wide range of design and operation parameters effect on the performance of regenerators was complicated.

Several analytical models of the heat (and possible mass) transfer occurring in rotary exchangers has been proposed in open literature, and are currently adopted in the design process of such devices. Lambertson and Montery [7] modelled the rotary heat exchanger as a counter flow one, neglecting the conductive resistance of the solid matrix and leakages effect. The original Lambertson and Montery formulation was limited to the case of equal thermal capacity streams, but was extended by Kays and London to the case streams of arbitrary heat capacities [8]. Kays and London summarized the basic

thermal design theory of the rotary regenerator which includes the effects of rotation, longitudinal and transverse conduction, pressure leakage, and carryover. Such formulation is currently the most widely used in the actual design process because detailed step−by−step solution procedures were outlined for rating (performance) and sizing (design) of counter−flow rotary regenerator. The $\epsilon - NTU_o$ method of analysis developed and Kays and London was used in the thermal design procedures of counter-flow regenerator. These summaries contain many design charts and design equations that allow a designer to predict the performance of sensible rotary heat exchangers under various operating conditions. Shah combined the charts and equations into a structured design methodology for sensible rotary heat exchangers and in [9] investigated the effects of carry-over leakage on the regenerator performance. Büyükalaca and Yilmaz [27] used numerical solution to evaluate the effect of rotation on the regenerator performance, validating their results with experimental data. Ghodsipour and Sadrameli [28] numerically investigated the effect of non−dimensional parameters on thermal effectiveness of regenerator, concentrating on rotational and flows speeds. Some experimental data, only loosely correlated to the computational set up, were also provided. Skiepko and Shah [10] compared the theoretical results and empirical data obtained from a large power plant regenerator. Due to the difficulties of measurement in a large scale industrial environment, however, experimental data show large uncertainty levels. Wu et al. [15] presented a numerical model for thermal and flow analysis of regenerator matrix, and investigated the effect of matrix rotation speed on the theoretical and empirical effectiveness. Sphaier and Worek [17] investigated the effect of axial diffusion within the porous substrate in a desiccant wheel and determined the conditions that allow to neglect this effect. Then in [18] they compared efficiency with a model 2−D and 1−D and in [19] presented a generalized methodology for analyzing heat and mass transfer regenerators. It is important to point out that, in general, the fluid dynamic problem within the single channel of a rotary heat exchanger is rather simple, and often easily predictable, as a laminar fully developed flow through a straight duct, although of non circular cross section. On the other hand, the actual performances of the device are strongly influenced by several phenomena taking place outside the wheel itself: undesired mixing of fluids, leakages, non uniformity in both inlet and outlet flows are just some examples. It is, thus, highly recommendable to decouple the analysis of the wheel volume and that of the outside flow.

In the operation of the sensible wheel, excess water and freezing on the matrix should be avoided. This is because excess water could result in leakage and undesirable mold growth while freezing could lead to poor performance by blocking the matrix .

2.3.2 Enthalpy − Desiccant wheel

The wheel rotates continuously between the supply air and exhaust air stream (regenerative air stream). In the enthalpy recovery, the wheel operates differently in summer and winter due to different operation conditions. In the summer, excess heat and moisture would be transferred to the exhaust to cool and dehumidify the supply air. In winter, heat and humidity would be recovered from the exhaust air stream.
As a result of the above discussion, the wheels are classified into two different types based

on its operation:

- the sorption wheels (desiccant rotary dehumidifiers) in which the emphasis is on air drying: this requires the use of external heat source to regenerate the desiccant;
- the enthalpy wheels focus on the energy exchange (sensible and latent energy) between the air streams and use no external source for regeneration of the desiccant.

In addition, the rotational speed ot the enthalpy wheel (5−20 RPM) is an order of magnitude higher than that of the desiccant wheel (0.1− 0.01 RPM).
There have been many works in modelling heat and moisture transfer in desiccant wheels. To predict the behaviour of enthalpy wheels, the fundamental governing equations have been solved numerically in [14], [20], [21], [22], but all these models present a computational domain of a channel of the wheel (Fig.2.8).

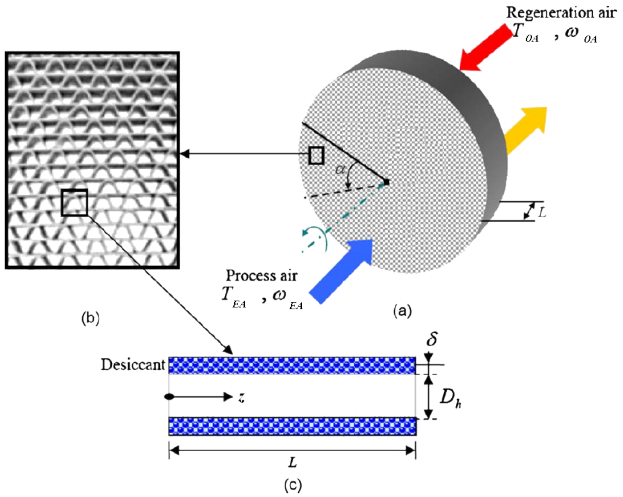

Figure 2.8: Numerical model focused in the flow inside the channel

Alternatively the use of heat and mass transfer analogies are available to predict the performance of enthalpy wheels. Recently, some useful correlations for sensible, latent and total effectiveness of enthalpy wheels were proposed ([11],[12],[29]), however they are still complex and need many addidional data. In particular Simonson and Besant ([11],[12]) published a series of papers in modeling the heat and mass transfer in a rotary energy wheel with tubular flow path. They developed a numerical model for a coupled heat and moisture in the rotary energy wheel. Their model is one dimensional, transient, and is formulated using the finite volume method with an implicit time discretization. The accuracy of the model has been confirmed using experimental data. The agreement between the measured and simulated effectiveness (sensible, latent, and total energy) was close and within the experimental uncertainty. These correlations, however, have a set of empirical parameters determined from the experimental data set, therefore, fail to

predict behavior in new solutions of both size and materials. So in the rapid evolution in the use of new materials and construction solutions, these correlations have limited use for new products.

3

Rotary exchangers design

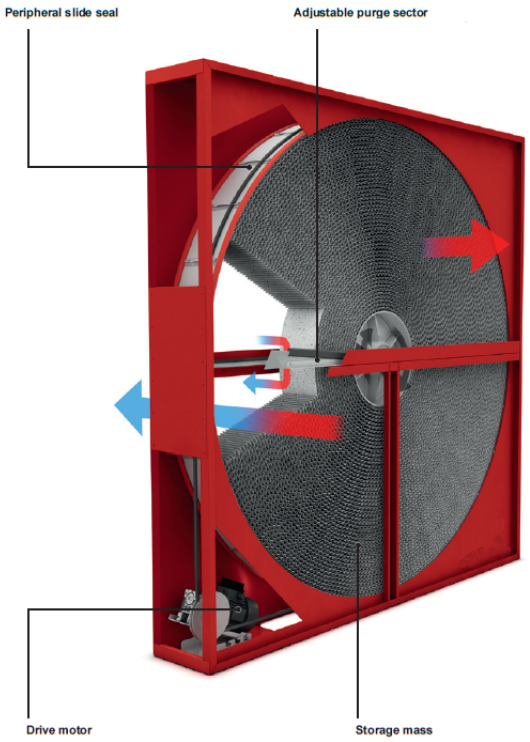

Figure 3.1: Schematic case of rotary exchanger

The more common air−to−air rotary energy wheel configuration is a counter−flow balanced and symmetric wheel. It is a rotating cylindrical wheel of length L and diameter D and it is divided into two equal sections: supply and exhaust section. While the wheel is rotating equal mass flow supply and exhaust air−streams are supplied to the wheel in a counter-flow arrangement.

3.1 The casing of a rotary exchanger

There are different casing designs, depending on the wheel diameter (D) and whether the wheel is one piece or segmented. The casing of a rotary exchanger is generally the metal (steel or aluminium) structure that houses the rotor. Cassettes are of punched sheet metal panellized construction. Self−supporting aluminium sheet steel casing are standard for single−component wheels with diameters (D) up to 2500 mm. A profile design of aluminium is used for wheels above 1500 mm diameter. The casing is extremely stable and the dimensions are flexible. The plate covers can be removed and replaced quickly and easily, a factor which is important for installation of segmented wheels. The height and width of the profile casing is limited to 4.2 m to reduce the problems of transport. Larger casings (welded construction, galvanised) are available customised for specific systems. Sometime rotary heat exchangers with coated casings are available for applications with very high hygiene requirements (e.g. hospitals): galvanized aluminium sheet steel, powder-coated.

The casings are designed for installation in a ventilation unit,the sides are open: this allows inspection and maintenance as required. On the other hand, the side walls of the casings in rotary heat exchangers with ducts can be enclosed when there are made suitable for the duct connection.

For transportation easiness, rotors are divided or segmented above a housing-size of 2500 mm (Fig. 3.2). Smaller rotors can also be segmented on request. The rotors provided with spokes are welded on the inside at the hub and on the outside with a cross-strut. This design offers the matrix a firm seat and prevents dirt ingress or condensate being created in zones where no flow exists.

Brush seal

Brush seal are used for both the circumferential seal and the inner seal in the cassettes. They are constructed of nylon brush and configured to seal against the enthalpy wheel band in the case of the circumferential seal, and against the wheel face in the case of the inner seal. These seals are full contact seals, have an integral clip, and they are clipped to the cassette face panel cut out (circumferential) or to the (inner) post. Constant−force springs permanently press the abrasion-resistant ring seal against the casing. This system (patent pending) minimises leakage and allows the ventilation unit to be sized for smaller air flow rates.

Purge sector

As energy recovery wheel rotates from the exhaust air stream into the supply air stream, a small amount of the exhaust air is traversing the flutes of the wheel media as it passes by the seal separating the two air streams. If this volume of exhaust air were allowed to mix with the clean supply air stream, "cross-contamination" would occur. Cross-contamination is virtually eliminated by a "purge section", which is an integral part of the casing design. The purge section utilizes the pressure difference which exists between

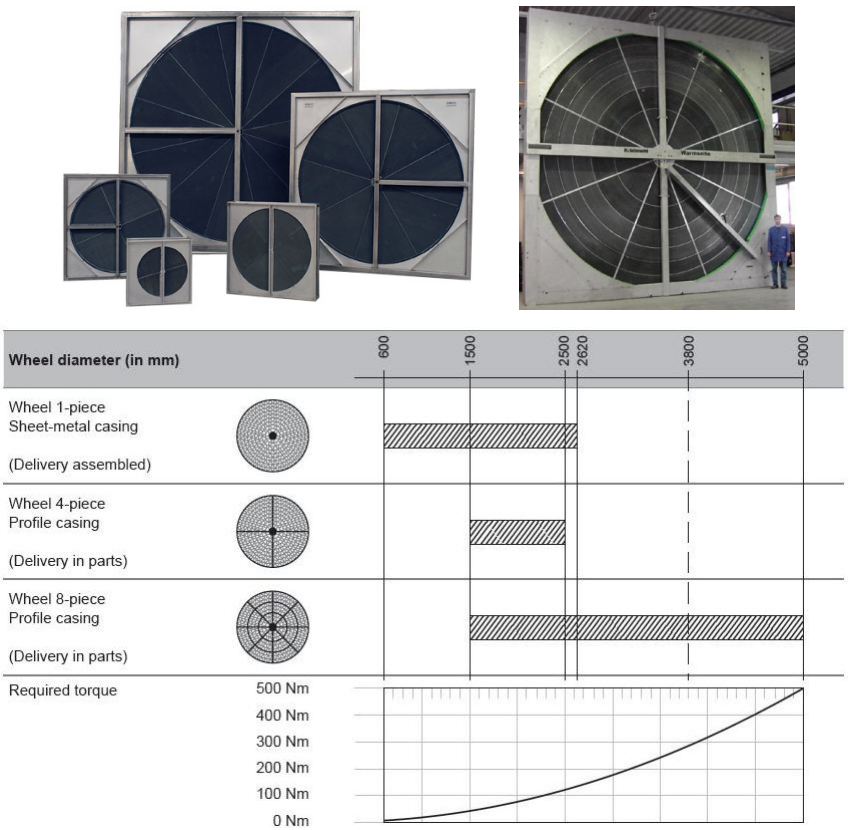

Figure 3.2: Designs and wheel dimensions for standard casing

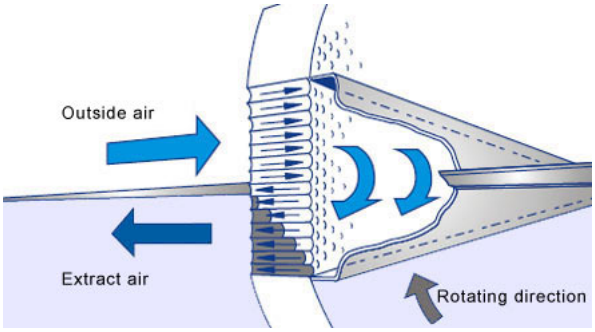

Figure 3.3: Schematic of purge sector operation

the outdoor and return air streams to purge the transfer media with clean outdoor air prior to its rotation into the supply air stream. Fig.3.3 provides a graphic representation

of the purge section operation. The purge section is adjustable. This allows for optimizing the required purge volume during system start−up, regardless of the pressure difference between the outdoor and return air streams (provided that the return air pressure is lower than that of the outdoor air).

Fan location options

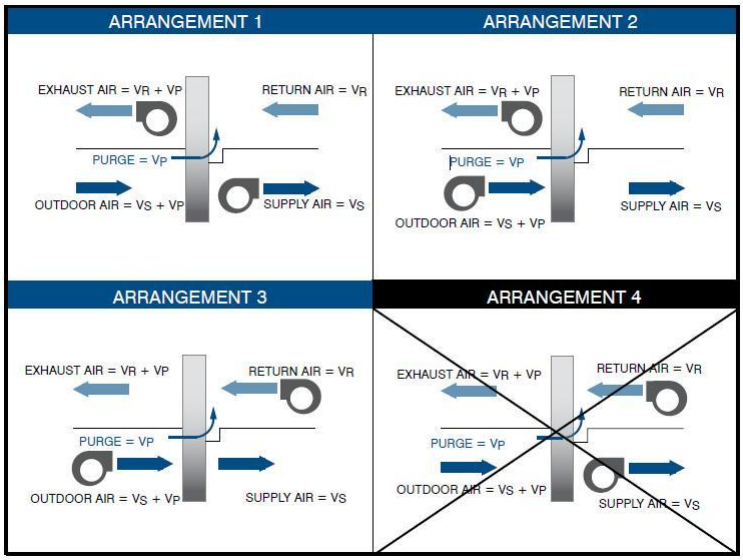

Figure 3.4: Fan arrangements for proper purge operation

Pressurization is critical to minimize crossover from exhaust to supply and to allow the purge to operate. To assure effective purge operation and limit cross-contamination, the pressure of the return air stream must be lower than that of the outdoor air stream. As shown in Fig. 3.4, three fan locations allow for effective purge operation. The fourth fan arrangement, draw−through supply and blow−through exhaust, must not be utilized if cross-contamination is of concern. In that arrangement the pressure of the exhaust side will always be greater than that of the return air and the purge section will not operate under such conditions. The purge and seal leakage air volume must be added to the appropriate fan(s) depending on the fan arrangement. Fig. 3.4 shows which fans must be sized to handle this additional air volume (Vp) for the different fan arrangements.

Motor

The wheel is driven by an electric motor and belt. The motor is generally fastened on the left or right on a rocker in the casing. Function is to provide the engine torque to the rotor (3.2). The rotation speed of the rotor for sensitive or enthalpy wheels range from

5 to 20 RPM . Speed of rotation are taken to significantly lower the desiccant wheels: some revolutions per hour.

Two versions of motor are available:

- Constant rotational speed: the motor is switched on and off by a single switch or contact. Output regulation (i.e. changing the heat recovery rate or moisture recovery rate) is not possible;
- Variable rotational speed the drive motor is controlled by a control unit. A frequency converter is generally used. Common additional functions are speed monitoring (by inductive sensors) and intermittent operation. If heat recovery is not required, the wheel is moved slightly at intervals to prevent dirt build-up. The control unit and as a result the wheel are normally actuated by the room temperature controller, for which the rotary heat exchanger is perceived as an energy resource for both heating and cooling, which forms part of the cascade control concept.

3.2 The wheel

The dimensional parameter that mainly characterizes the heat exchanger in the market is the diameter of the rotor (D). Depending on the needs of both technical and functional, rotary heat exchangers are designed and sized: measurements of the diameter commercially available in the market for this type of exchanger range from 500 mm to $5000-6000\ mm$.

Storage matrix

Various combinations of substrates, chemicals, synthesizing processes and design features are commercialy available depending upon the application. The typical substrate for the storage matrix are: aluminium foil, stainless steel foil , tissue paper, plastic sheet, active carbon paper, glass fibre paper, metal silicate loaded paper, ceramic fibre paper.

Figure 3.5: Different matrix material used in the rotary exchangers

A corrugated and a smooth foil are wound together as the storage mass. This forms triangular (or trapezoidal, sinusoidal) axial ducts.

Depending on the application, the solid foils are 60 μm to 120 μm thick (t in Fig. 3.7). The different material thickness of metal foil is used for:

- $t = 60[\mu m]$ air handling systems with moderate polluted exhaust air;
- $t = 70[\mu m]$ (standard) air handling systems with moderate polluted exhaust air, qualified for high pressure cleaning;
- $t = 100[\mu m]$ rotary with frequent high pressure cleaning and special demand on durability;
- $t = 120[\mu m]$ special rotary heat exchanger, for example in laquer plants.

The width of the rotor (L) is 200 mm for most commercial air conditioning applications: industry applications can require width of 300 mm, while in the small domestic installations mainly involve 100 mm wide wheels. This parameter affects the heat exchanger pressure losses and the effectiveness.

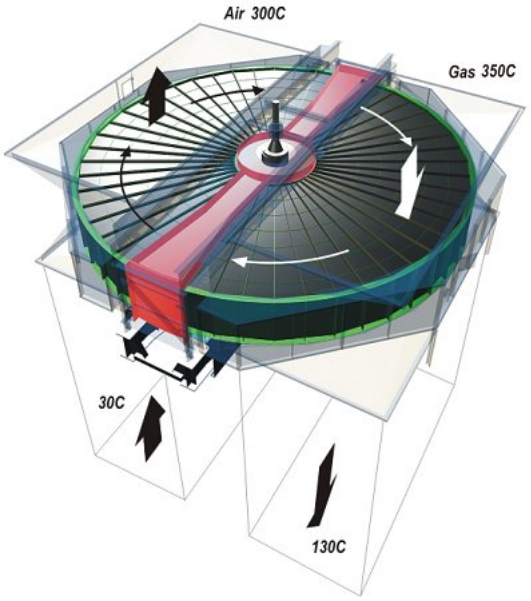

Figure 3.6: Industry application of rotary exchangers

Channels

Rectangular, triangular, or sinusoidal shapes of matrices can be made but the main parameter that characterizes the channel is the height of the waves (l_h in Fig. 3.7).

The different corrugation height is used for:

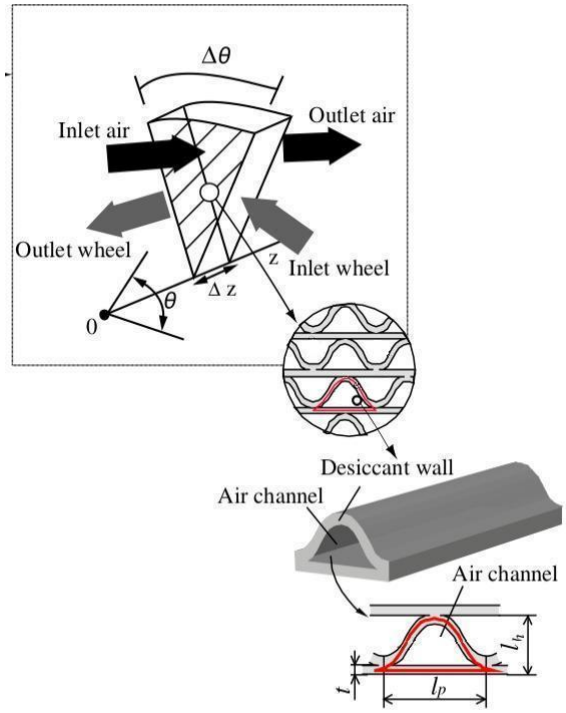

Figure 3.7: Schematic of a channel in the matrix wheel

- $l_h = 1.50 - 1.70[mm]$ high efficiency due to tight exchanger, but also increased pressure drop;
- $l_h = 1.90 - 2.00[mm]$ (standard) air handling systems with moderate polluted exhaust air;
- $l_h = 2.50 - 3.00[mm]$ special design for more polluted exhaust air or indutrial applications of heat recovery.

The channel pitch (l_p in Fig. 3.7) is a parameter imposed by the method of corrugation: as the wave is typically produced through the stretching of a flat sheet into two toothed rollers to allow the exit of the teeth of the roller, the wave pitch is determined if the height is fixed ($l_p \cong 2l_h$). However, with other methods of production (e.s.: molding) you can vary this ratio and therefore change the matrix porosity.
The porosity (ϕ) of the matrix is the ratio of the fluid (generally air) stream volume V_f to the total (fluid V_f+ solid matrix V_m) volume V_{tot} and can be written as:

$$\phi = \frac{V_f}{V_f+V_m} = \frac{V_f}{V_{tot}} \text{ or } \frac{V_m}{V_{tot}} = (1-\phi)$$

.

The porous matrix is used in order to increase the available surface area A for heat and mass trasnfer. The density area or volumetric surface area $\frac{A}{V_{tot}}$ is used to describe the compactness of the wheel.

3.3 Operation conditions in the channels

The corrugated sinusoidal duct geometry is the most common in honeycomb wheels, due to simplicity of construction and large surface area. The cross−sectional geometry of a corrugated duct is shown in Fig. 3.7. It is observed the the singhe tube can be approximated with a sine curve for the upper portion and straight line (or arc) for the lower portion.

The actual velocity of the fluid in the channels in z−direction is $\widetilde{w_i} = \dot{V}_i/(\phi S_{fi})$ where the $\dot{V}_i$ is the volumetric flow rate of fluid $[\frac{m^3}{s}]$ in the section i of the wheel.
The flow speed v in feeding and outlet wheel manifolds is from 0.5 to 5.0 $[m/s]$.
Given the geometrical narrowing of the duct section to the section of rotary exchanger like

$$\phi_{Di} = \frac{\vartheta_i \pi (\frac{D}{2})^2}{S_{duct_i}} \ ,$$

the velocity in the channels can be written as $\widetilde{w_i} = \frac{v_i}{\phi_{Di}\phi}$. In general the i section of the wheel and duct can be different.

The hydraulic diameter (d_h) is a commonly used parameter for comparing flow in noncircular tubes and channels: $d_h = \frac{4A}{P}$ where A is the cross sectional area and P the wetted perimeter of the cross-section.
To calculate the hydraulic diameter of a sinusoidal duct you can calculate the cross area and perimeter, or use the following equation ([30]):

$$d_h = l_h\Big[1.0542 - 0.4670\big(\tfrac{l_h}{l_p}\big) - 0.1180\big(\tfrac{l_h}{l_p}\big)^2 + 0.1794\big(\tfrac{l_h}{l_p}\big)^3 - 0.0436\big(\tfrac{l_h}{l_p}\big)^4\Big].$$

For the most common range for l_h and l_p, we get $d_h = 0.58 \div 2,48[mm]$.
Considering the thermodynamic properties of the fluid at the average operating temperature (for example, air at 20°C) and the crossing speed of channels, we obtain the following range for the dimensionless number Reynolds inside the channels:

$$Re = \frac{\rho_f d_h \widetilde{w_i}}{\mu_f} = 20 \div 800.$$

In such small diameter ducts, laminar flow prevails and the entrance effect can be neglected. Distributed pressure losses and heat transfers of laminar flow have been extensively studied for regularly shaped ducts and also with some irregular geometry ([31]). Interpolating the values in the Table 3.1([31]) for the various geometries of the channels, we can find the values used to describe the pressure drop and heat exchange iin the channels.

The pressure drop ΔP through honeycomb structures consists of the parts : local pressure loss (inlet and outlet) ΔP_{io} and frictional pressure loss ΔP_f:

Shape	l_h/l_p	fRe	Nu_T
Circular	1.0	16.081	3.672
Square	1.0	14.115	3.001
Elliptic	0.5	16.941	3.766
Sine	2.0	14.576	2.658
Sine	1.5	13.934	2.614
Sine	1.0	12.922	2.463
Sine	0.75	12.326	2.317
Sine	0.5	11.173	2.135

Table 3.1: fRe and Nu_T of fully developed laminar flow for some ducts

$$\Delta P = \Delta P_{io} + \Delta P_f$$

Local pressure loss ΔP_{io} can be calculated from

$$\Delta P_{io} = K_{io} \frac{\rho_f \tilde{w}^2}{2}$$

where K_{io} is the loss coefficient due to a sudden contraction and a sudden expansion at the inlet and outlet of the sample respectively. It is only related to the geometrical parameters of the wheel as a function of wheel's porosity ϕ: when ϕ increases from zero to unit, K_{io} decreases continuously from 1.5 to zero ([32]).
Delivered pressure loss ΔP_f can be calculated from

$$\Delta P_f = 4f \frac{L}{d_h} \frac{\rho_f \tilde{w}^2}{2}$$

where f is the Fanning friction factor calculated from table 3.1.

With current general conditions, the economically optimal values for wheels are $\Delta P = 80 \div 200[Pa]$. However, to reduce costs, more and more heat recovery units whose pressure drops are above these economically reasonable values are being installed. This affects the feasibility of the system. Heat recovery causes pressure drop gall to the result a decrease in operating costs for air conditioning by using fresh air from exhaust air conditions.

Using the Nussel number Nu_T in table 3.1, you can evaluate the convective heat trasfer coefficient $h = \frac{Nu_T k}{d_h}$ where k is the termal conductivity of the fluid estimated to average operation conditions.

The fluid flow inside the channels is therefore determined.

4

Numerical model for sensible rotary exchangers

The model here proposed does not require the detailed modelling of individual channels, whose performance are summarized in terms of distributed sources based on the local values of temperature and heat transfer coefficients and friction within the channel deduced from open literature [31, 33]. This allows for a coarse grid in the wheel discretization, without loss of generality. Leakages and non-uniformity either in the flow or in the wheel, as an example, could be easily simulated, as the model is simple an efficient enough to be incorporated within larger CFD models for the calculation of an actual complete system, as in [16].

4.1 Mathematical Model

The computational domain covers the whole wheel, as in Fig.2.3, z is oriented along the axes of rotation. Cartesian, rather than cylindrical, coordinates are used in order to allow easy incorporation in a larger model for the whole recuperating system, including ducting, which usually is not axisymmetric.

The development of the mathematical model describing the heat and fluid flow in the rotary regenerator is based on the following simplifying assumptions:

1. the regenerator operates with constant mass flow rates, rotation speed and inlet temperatures for both fluids;
2. there are no thermal energy sources or sinks within the regenerator walls or fluids;
3. no phase change occurs in the regenerator;
4. the flow is incompressible, with negligible viscous dissipation;
5. constant properties fluids are considered;

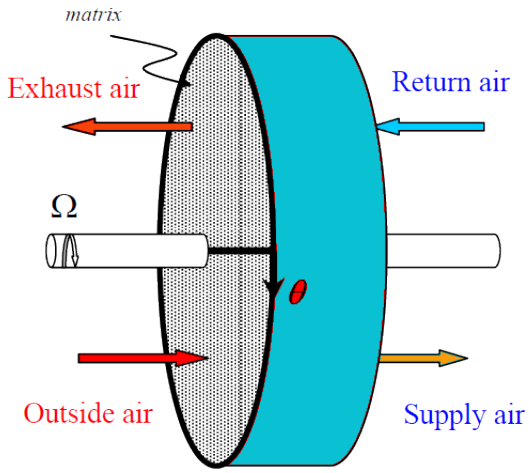

Figure 4.1: Schematic of the rotary regenerator

6. the wall/fluid convection heat transfer coefficient h is independent on the temperature and time;

7. rotating speed is slow enough to neglect wheel mechanical work production;

8. the system is globally adiabatic, i.e. the heat transfer occurs only among the two fluids and the solid matrix;

In addition, in the present computation we will focus on uniform inlet and outlet distributions of equal thermal capacity flows, leading to uniform heat transfer coefficient within the whole wheel. However, the model is not limited to such conditions, and can handle different boundary conditions.

The energy equation for the fluid can thus be written as:

$$\rho_f c_{pf} \phi \left(\frac{\partial \widetilde{T_f}}{\partial \widetilde{t}} + \widetilde{u} \frac{\partial \widetilde{T_f}}{\partial \widetilde{x}} + \widetilde{v} \frac{\partial \widetilde{T_f}}{\partial \widetilde{y}} + \widetilde{w} \frac{\partial \widetilde{T_f}}{\partial \widetilde{z}} \right) =$$
$$k_f \phi \left(\frac{\partial^2 \widetilde{T_f}}{\partial \widetilde{x}^2} + \frac{\partial^2 \widetilde{T_f}}{\partial \widetilde{y}^2} + \frac{\partial^2 \widetilde{T_f}}{\partial \widetilde{z}^2} \right) + h \frac{A}{V} (\widetilde{T}_w - \widetilde{T_f}) \tag{4.1.1}$$

In eq.(4.1.1) tilde identifies dimensional quantities, and ϕ is a porosity coefficient given by the ratio between the fluid passage actual cross-section and the wheel front area. The vertical velocity w is the actual velocity inside each channel; for uniform inlet flow i, where i can be either hot stream h or cold stream c, this is given by:

$$\widetilde{w_i} = \dot{V}_i / \phi S_{fi} \tag{4.1.2}$$

where S_{fi} is the wheel from area exposed to fluid i. If the solid matrix is composed by vertical channels, the radial velocities are imposed only by the wheel rotation. This may be a good approximation even for porous rotors, due the negligible pressure gradient induced by the slow rotation speed:

$$\widetilde{u} = -r\omega \sin\vartheta = -\omega\widetilde{y} \qquad \widetilde{v} = r\omega\cos\vartheta = \omega\widetilde{x} \tag{4.1.3}$$

For a constant properties material, the energy equation for the solid matrix can be written as:

$$\rho_w c_w (1-\phi)\left(\frac{\partial\widetilde{T_w}}{\partial\widetilde{t}} + \widetilde{u}\frac{\partial\widetilde{T_w}}{\partial\widetilde{x}} + \widetilde{v}\frac{\partial\widetilde{T_w}}{\partial\widetilde{y}}\right) =$$
$$k_w(1-\phi)\left(\frac{\partial^2\widetilde{T}_w}{\partial\widetilde{x}^2} + \frac{\partial^2\widetilde{T}_w}{\partial\widetilde{y}^2} + \frac{\partial^2\widetilde{T}_w}{\partial\widetilde{z}^2}\right) + h\frac{A}{V}(\widetilde{T_f} - \widetilde{T}_w) \tag{4.1.4}$$

where $\widetilde{w} = 0$, while $\widetilde{u}$ and $\widetilde{v}$ are equal to the corresponding fluid velocity components. Thermal conductivity in eq.(4.1.4) is assumed isotropic, as the following results will demonstrate that anisotropy has negligible effect.

Finally, it is important to note that the Equations (4.1.1) and (4.1.4) are coupled because of the convection term that appears, with opposite sign, at the right side of both equations.

4.2 Non − Dimensionalization

Different choices of relevant non dimensional parameters can be found in literature. Here, we chose, as reference parameter, the axial length L of the wheel and the rotation period $t_0 = 2\pi/\omega$. Temperature is non-dimensionalized with respect to the difference between cold fluid inlet temperature $\widetilde{T}_c^0$ and hot fluid inlet temperature $\widetilde{T}_h^0$:

$$T = \frac{\widetilde{T} - \widetilde{T}_c^0}{\widetilde{T}_h^0 - \widetilde{T}_c^0} \tag{4.2.1}$$

We can also introduce the Fourier numbers, measure of the ratio between conductive and convective heat flux, for the two fluids and the matrix

$$Fo_f = \frac{k_f}{\rho_f c_{pf}}\frac{t_o}{L^2} \qquad Fo_w = \frac{k_w}{\rho_w c_w}\frac{t_o}{L^2} \tag{4.2.2}$$

and the ratio R between the time required by the fluid to run through the wheel length L and the rotation period t_0:

$$R = \widetilde{w}\frac{t_o}{L} \tag{4.2.3}$$

Finally, the usual number of thermal units NTU and non-dimensional capacities are defined as

$$NTU = \frac{hA}{C} = \frac{hA}{\dot{m}c_{pf}} \tag{4.2.4}$$

$$C_r^* = \frac{C_r}{C_{min}} = \frac{M_w c_w}{(\dot{m}c_{pf})_{min} t_0} \tag{4.2.5}$$

In general, we can have different fluids, different mass flow rates, and different cross section for each stream i. In such case, we will have two different set of parameters for hot and cold stream: Fo_{fh}, R_h, NTU_h, C_c, C_{rh}^* and Fo_{fc}, R_c, NTU_c, C_c, C_{rc}^*. Thus, the capacity ratio is defined as:

$$C^* = \frac{C_{min}}{C_{max}} \qquad C_{min} = min(C_c; C_h) \qquad C_{max} = max(C_c; C_h) \tag{4.2.6}$$

A global number of thermal units can also be defined as

$$NTU_o = \left[\frac{1}{C_{min}}\right]\left[\frac{(hA)_c(hA)_h}{(hA)_h + (hA)_c}\right] \tag{4.2.7}$$

Finally, using L/t_0 as reference velocity, the non dimensional flow velocity components become:

$$u = -2\pi y \qquad v = 2\pi x \qquad w = R \tag{4.2.8}$$

and Eqs. (4.1.1) and (4.1.4) reduce to the following form:

$$\frac{\partial T_f}{\partial \theta} + u\frac{\partial T_f}{\partial x} + v\frac{\partial T_f}{\partial y} + w\frac{\partial T_f}{\partial z} =$$
$$Fo_f\left(\frac{\partial^2 T_f}{\partial x^2} + \frac{\partial^2 T_f}{\partial y^2} + \frac{\partial^2 T_f}{\partial z^2}\right) + NTU \cdot R(T_w - T_f) \tag{4.2.9}$$

$$\frac{\partial T_w}{\partial \theta} + u\frac{\partial T_w}{\partial x} + v\frac{\partial T_w}{\partial y} =$$
$$Fo_w\left(\frac{\partial^2 T_w}{\partial x^2} + \frac{\partial^2 T_w}{\partial y^2} + \frac{\partial^2 T_w}{\partial z^2}\right) + \frac{NTU}{C_r^*}(T_f - T_w) \tag{4.2.10}$$

In eq.(4.2.9), in general, Fo_f, R and NTU will assume different values in the hot and cold section.

4.3 Boundary Conditions

In the present computations inlet fluid temperature, as well as the two stream velocities, are assumed constant. No explicit thermal boundary condition is required in the outlet section, while the outer shell surface is assumed adiabatic. Thus, the complete set of fluid boundary conditions for the fluid equations is defined by

$$T_h^0 = 1 \qquad T_c^0 = 0$$

on hot stream and cold stream inlet respectively, and

$$\frac{\partial T_f}{\partial n} = 0$$

on the lateral surface of the wheel.

Under the assumption of globally adiabatic device, in the solid matrix heat transfer occurs only between the internal channel surfaces and the fluid, and is modelled by the the source terms. All of the external surfaces of the domain are thus assumed adiabatic:

$$\frac{\partial T_w}{\partial n} = 0 \tag{4.3.1}$$

Although the solid appears to be solved with Neumann condition on all of the boundaries (eq.4.3.1), the problem (4.2.9) and (4.2.10) is well posed, since the convection source term offers the required coupling and constraint on the solid matrix temperature.

4.4 Performance parameters

If an averaged outlet bulk temperature at each wheel cross section is defined (for each fluid i, $i = h, c$) as in the following:

$$T_{bi} = \frac{\int_{S_{outlet}} w_i T_{fi} dS}{\int_{S_{outlet}} w_i dS} = \frac{1}{S_{outlet}} \int_{S_{outlet}} T_{fi} dS \tag{4.4.1}$$

we can obtain the regenerator effectiveness from outlet bulk temperatures:

$$\epsilon = \frac{q}{q_{max}} = \frac{C_h(T_h^0 - T_{bh})}{C_{min}(T_h^0 - T_c^0)} = \frac{C_c(T_{bc} - T_c^0)}{C_{min}(T_h^0 - T_c^0)}. \tag{4.4.2}$$

The maximum reference heat flux q_{max} would be attained for a perfect a counter-flow recuperator of infinite surface area, zero longitudinal wall heat conduction and no leakages.

Kays and London [8] proposed a popular correlation for ϵ. In particular, if ϵ_o is the effectiveness of a cross−flow heat exchanger, φ_r a correction factor for rotation speed and φ_c a correction factor for the cleaning region (purge sector), Kays and London suggest:

$$\epsilon = \epsilon_o \varphi_r \varphi_c \tag{4.4.3}$$

$$\epsilon_o = \frac{1 - e^{-NTU_o(1-C^*)}}{1 - C^* e^{-NTU_o(1-C^*)}} \tag{4.4.4}$$

$$\varphi_r = 1 - \frac{1}{9C_r^{*1.93}} \tag{4.4.5}$$

In the present computations we assume no cleaning region, i.e. $\varphi_c = 1$.

4.5 Numerical implementation

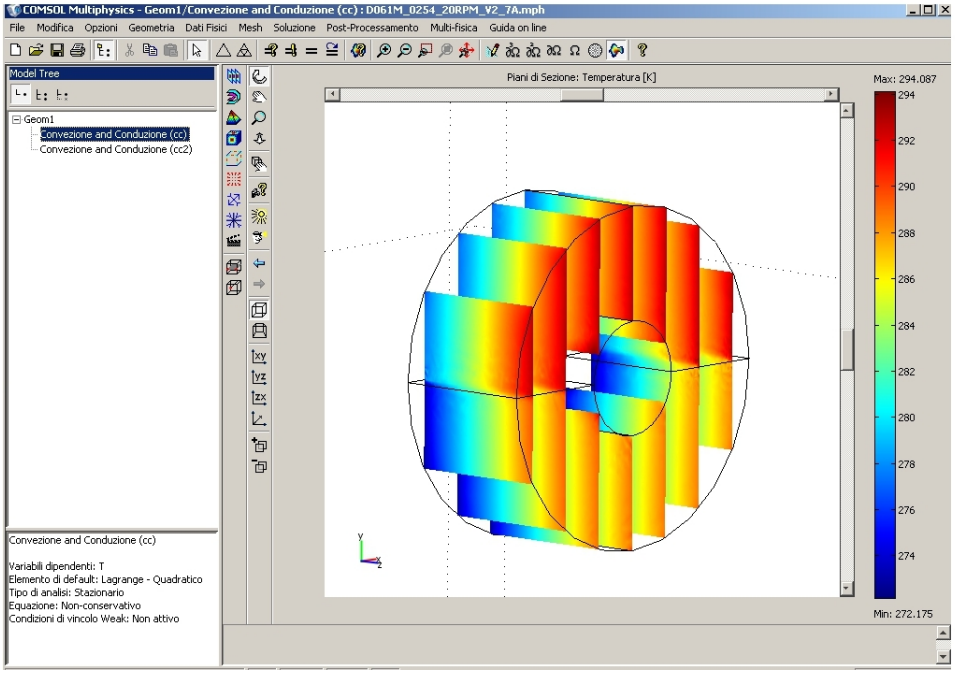

Figure 4.2: Screenshot of Comsol software sensible model

The equations of the model were discretized via COMSOL Multiphysics 3.5 software for the implementation of the FEM: we used a 3D unstructured mesh with only tetrahedral Lagrange - quadratic order elements.The resulting algebraic systems are solved via SPOOLES non iterative method and the convergence of the solution is reached fairly quickly.

Typical mesh has 30.000 elements, and a further increase of 40% elements yields less than 0.4% variation in the computed efficiency.

Operationally, the domain was divided into two subdomains depending on the fluid field: in this way in the two subdomains are solved the same equations but with the set non dimensional velocity $w = R$.

In Fig.4.2 we can see a screenshot of Comsol software post-processor: it refers to a simulation of a real recupatore with an internal diameter operating with a traverse speed of the fluid equal to 2.7 m / s and a rotation of 20 RPM.

4.6 Result and Discussion

The model accuracy was validated comparing the results with experimental reported in [34–36]. Sanaye [34] considered a wheel diameter of $D = 70cm$, length $L = 20cm$, and a rotational speed from 3 to $12rpm$. Sparrow et al. [35] provide data for a similarly sized wheel ($D = 61cm$, length $L = 25.4cm$, but with a large hub diameter of $20.3cm$. Finally, some results from an experimental campaign on similarly sized commercially available recuperators are considered [36]. All of the wheels are made of aluminium, and h is computed from laminar correlations, since here $Re < 2000$. Only qualitative comparisons were possible with data in [10, 28], since these sources do not provide all of the data required by the present model.

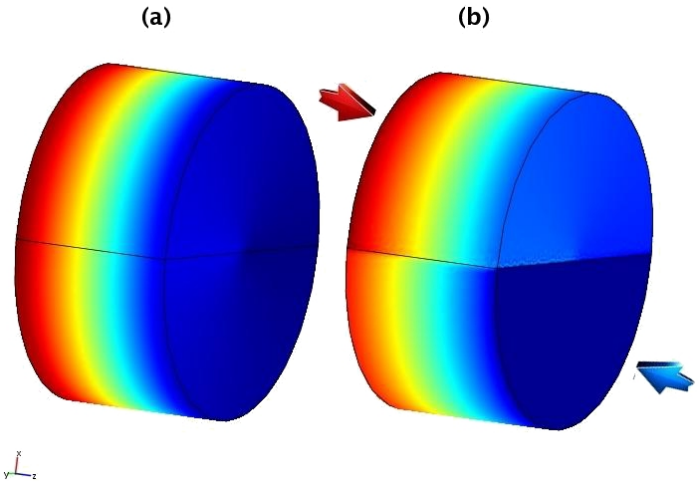

Figure 4.3: Temperature in 3D (a) matrix (b) fluid

In Fig.4.3 two typical temperature maps of solid (a) and fluid (b) domain are shown. The matrix has the effect of thermal inertia and storage: it is responsible for the exchange of thermal energy between the two fluid flows. The high conductivity of the solid matrix yields uniform solid temperature in the radial direction ,Fig.4.3(a), while we get a clear stratification in the axial direction. This suggest a negligible influence of radial solid conductivity, a possible significant effect of axial solid conduction, and a negligible influence

of the wheel diameter. Fig.4.3(b), as expected, shows a marked fluid temperature jump at junction between the hot and cold sectors.

Performance results are usually given as a function of NTU_o; however, it is worth noting that, for a fixed geometry, NTU_o and C_r^* are not independent. Thus, each set experimental data offers results along a line in the $NTU_o - C_r^*$ plane, as shown in Fig.4.4.

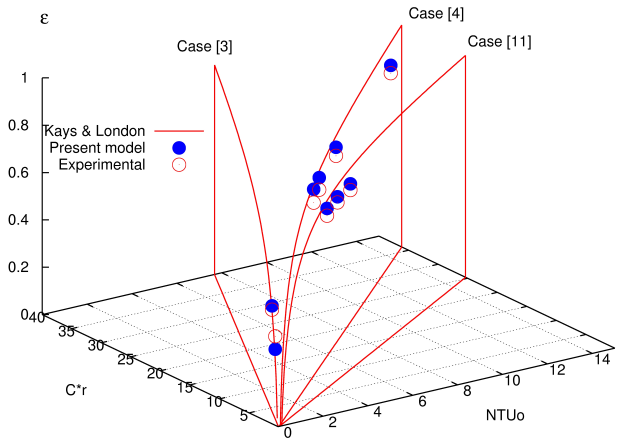

Figure 4.4: Efficiency as a function of NTU_o and C_r^*

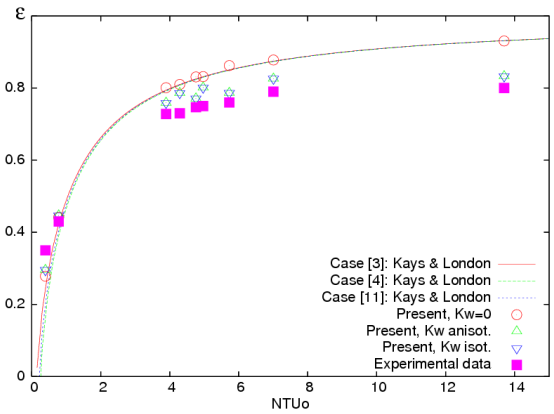

Figure 4.5: Model validation

Computed efficiency are compared in Fig.4.5. NTU_o is by far the most relevant parameter: the three different analytical curves from Kays and London, following the

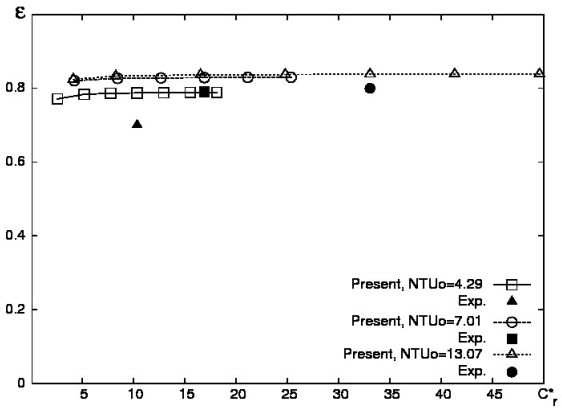

Figure 4.6: C_r^* influence

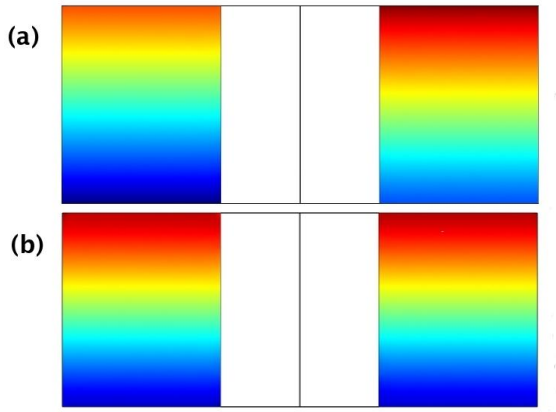

Figure 4.7: Temperature field in a meridional plane, neglecting hub conduction: (a), fluid; (b) solid matrix

different C_r^* related to the three different test cases, collapse into a single line: a minimum difference is detected only at very low values of NTU_o. As expected, our model is in good agreement with Kays and London if we neglect the axial conduction, but is remarkably more accurate when this effect is taken into account. This is more evident at higher values of NTU_o I.e., for a given geometry, at lower mass flows. As suggested by the temperature map analysis, radial conduction is negligible: thus, assuming an isotropic solid conductivity or a more accurate anisotropic model, taking into account the different topology of the solid matrix in the radial and axial direction, does not show any relevant effect.

The limited impact of C_r^* is further clarified in Fig.4.6: for any given value of NTU_o,

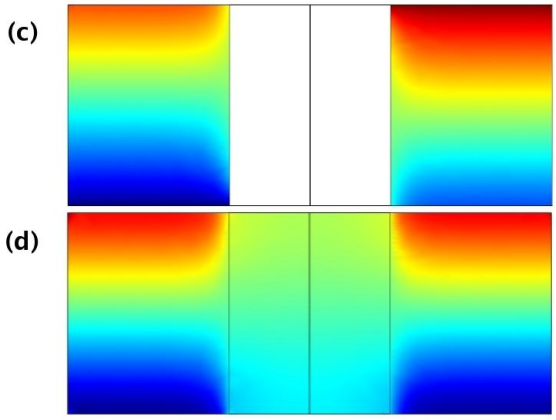

Figure 4.8: Temperature field in a meridional plane, with hub conduction: (c), fluid; (d) solid matrix

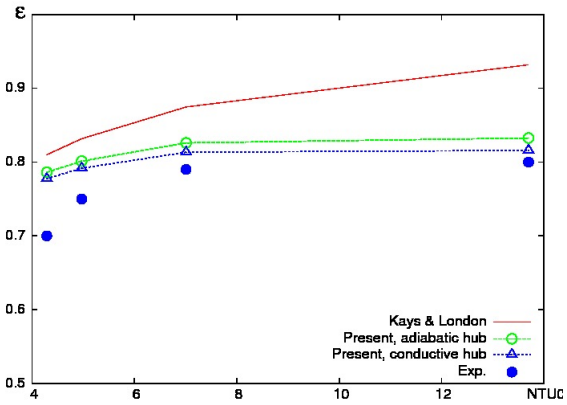

Figure 4.9: Hub effect on heat exchanger efficiency

the actual computed efficiency is nearly constant in a broad range of C_r^*.

4.6.1 Practical application: hub conduction effect

To assess the flexibility of the current model, the case presented by Sparrow et al.[35] is further analyzed. Their geometry, in fact, is characterized by a thick hub with no fluid passage. We can expect that such a solid hub could induce a concentration of heat flux in the axial direction, due to its higher conductivity with respect to the porous matrix. Such an effect cannot be easily handled by analytical and simplified model, since it will induce a non uniform temperature in the radial direction. In Fig.4.7 we show the temperature in the fluid (a) and solid (b) domain computed neglecting conduction through the hub,

on a meridional lane; Fig.4.8 shows the same temperature fields predicted including the solid hub conduction. The higher conductivity induce a nearly uniform temperature in the wheel core (Fig.4.8). The plot of recuperator efficiency in Fig.4.9 shows that the inclusion of the hub conductivity significantly improve the prediction accuracy.

4.7 Summary

A numerical model for the analysis of heat transfer in rotary recuperators is determined. The details of the pressure drop and convective heat transfer in the single matrix channels are simulated with distributed sources, assuming a value for the friction factor and heat transfer coefficient. However, these values may change from point to point. The model was validated against experimental data, and offers a significant improvement over traditional analytical approach. Furthermore, an application to a geometry characterized by a thick core hub, demonstrated that the model is flexible enough to take into account non standard geometries, which are not easily handled by traditional simplified approach and yet can significantly affect the heat exchanger performances.

This work was presented at the XXVII UIT Congress in 2008 ([37]).

5

Desiccant materials

5.1 Desiccant overview

Desiccant materials in the air−conditioning applications are defined by the capability of the material to adsorb and desorb water at a given temperature ([38]).

Adsorption (in the present context, positive adsorption at the gas/solid interface) is the enrichment of one or more components in an interfacial layer. *Physisorption* (as distinct from *chemisorption*) is a general phenomenon: it occurs whenever an adsorbable gas (the adsorptive) is brought into contact with the surface of a solid (the adsorbent). The intermolecular forces involved are of the same kind as those responsible for the imperfection of real gases and the condensation of vapours. In addition to the attractive dispersion forces and the short range repulsive forces, specific molecular interactions (e.g. polarisation, field-dipole, field gradient-quadrupole) usually occur as a result of particular geometric and electronic properties of the adsorbent and adsorptive.

It is convenient to regard the interfacial layer as comprising two regions: the *surface layer* of the adsorbent (often simply called the *adsorbent surface*) and the *adsorption space* in which enrichment of the adsorptive can occur. The material in the adsorbed state is known as the adsorbate, as distinct from the adsorptive, i.e. the substance in the fluid phase which is capable of being adsorbed.
When the molecules of the adsorptive penetrate the surface layer and enter the structure of the bulk solid, the term *absorption* is used. It is sometimes difficult, impossible or irrelevant to distinguish between *adsorption* and *absorption*: it is then convenien to use the wider term *sorption* which embraces both phenomena and to use the derived terms sorbent, sorbate and sorptive.
The term *adsorption* may also be used to denote the process in which adsorptive molecules are transferred to, and accumulate in, the interfacial layer. Its counterpart, *desorption*, denotes the converse process, in which the amount adsorbed decreases. Adsorption and desorption are often used adjectivally to indicate the direction from which experimentally determined adsorption values have been approached, e.g. the adsorption curve (or point) and the desorption curve (or point). Adsorption hysteresis arises when the adsorption and desorption curves do not coincide. The relation, at constant temperature, between

the amount adsorbed and the equilibrium pressure of the gas is known as the *adsorption isotherm*.
Many adsorbents of high surface area are porous and with such materials it is often useful to distinguish between the *external* and *internal surface*. The external surface is usually regarded as the envelope surrounding the discrete particles or agglomerates, but is difficult to define precisely because solid surfaces are rarely smooth on an atomic scale. A suggested convention is that the external surface be taken to include all the prominences and also the surface of those cracks which are wider than they are deep; the internal surface then comprises the walls of all cracks, pores and cavities which are deeper than they are wide and which are accessible to the adsorptive . In practice , the demarcation is likely to depend on the methods of assessment and the nature of the pore size distribution. Because the accessibility of pores may depend on the size and shape of the gas molecules, the area of, and the volume enclosed by, the internal surface as determined by gas adsorption may depend on the dimensions of the adsorptive molecules (molecular sieve effect). The roughness of a solid surface may be characterized by a roughness factor, i.e. the ratio of the external surface to the chosen geometric surface. In the context of physisorption, it is expedient to classify pores according to their sizes:

- pores with widths exceeding about 50 nm (0.05 pm) are called *macropores*;
- pores of widths between 2 nm and 50 nm are called *mesopores*;
- pores with widths not exceeding about 2 nm are called *micropores*.

These limits are to some extent arbitrary since the pore filling mechanisms are dependent on the pore shape and are influenced by the properties of the adsorptive and by the adsorbent−adsorbate interactions. The whole of the accessible volume present in micropores may be regarded as adsorption space and the process which then occurs is micropore filling, as distinct from surface coverage which takes place on the walls of open macropores or mesopores. Micropore filling may be regarded as a primary physisorption process; on the other hand, physisorption in mesopores takes place in two more or less distinct stages (monolayer-multilayer adsorption and capillary condensation).
In monolayer adsorption all the adsorbed molecules are in contact with the surface layer of the adsorbent. In multilayer adsorption the adsorption space accommodates more than one layer of molecules so that not all adsorbed molecules are in direct contact with the surface layer of the adsorbent. In capillary condensation the residual pore space which remains after multilayer adsorption has occurred is filled with condensate separated from the gas phase by menisci. Capillary condensation is often accompanied by hysteresis.

The desiccant materials are characterized mainly by their adsorption isotherm shape. At a given temperature, the relationship between the amount adsorbed by unit mass matrix and the equilibrium pressure is defined as adsorption isotherm. The adsorption isotherm is typically presented in graphic format in the case of experimental studies. Brunauer [39] gather experimental data isotherms of gas solid systems and grouped them into five categories, as shown in Fig 5.1: p/p^o is the pressure divided by the vapor pressure for the dessicant material at that temperature and the *Specific amount*

adsorbed is normalized with the maximum amounts absorbed by the desiccant material at that temperature.

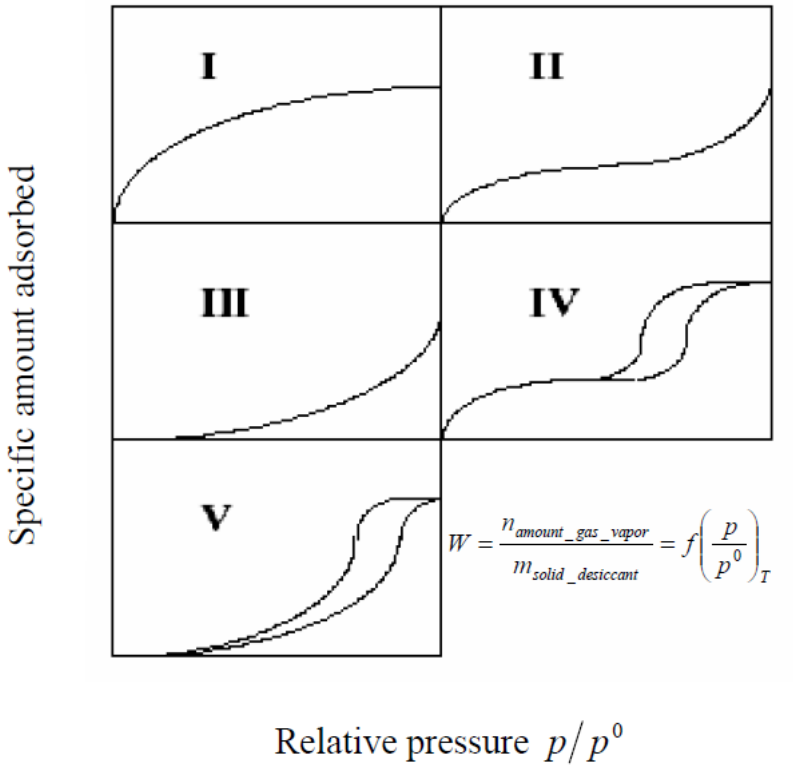

Figure 5.1: The Brunauer classification of gas physisorption isotherm

The reversible Type I isotherm is concave to the p/p^o axis and a approaches a limiting value as p/p^o1. Type I isotherms are given by microporous solids having relatively small external surfaces (e.g.activated carbons, molecular sieve zeolites and certain porous oxides), the limiting uptake being governed by the accessible micropore volume rather than by the internal surface area.

The reversible Type II isotherm is the normal form of isotherm obtained with a non-porous or macroporous adsorbent. The Type II isotherm represents unrestricted monolayer-multilayer adsorption. The inflection point, the beginning of the almost linear middle section of the isotherm, is often taken to indicate the stage at which monolayer coverage is complete and multilayer adsorption about to begin.

The reversible Type III isotherm is convex to the p/p^o axis over its entire range and therefore does not exhibit an inflection point. Isotherms of this type are not common,

but there are a number of systems (e .g. nitrogen on polyethylene) which give isotherms with gradual curvature and an indistinct inflection point .In such cases , the adsorbate-adsorbate interactions play an important role.

Characteristic features of the Type IV isotherm are its hysteresis loop, which is associated with capillary condensation taking place in mesopores, and the limiting uptake over a range of high p/p^o . The initial part of the Type IV isotherm is attributed to monolayer-multilayer adsorption since it follows the same path as the corresponding part of a Type II isotherm obtained with the given adsorptive on the same surface area of the adsorbent in a non-porous form.

Type IV isotherms are given by many mesoporous industrial adsorbents. The Type V isotherm is uncommon; it is related to the Type III isotherm in that the adsorbent-adsorbate interaction is weak, but is obtained with certain porous adsorbents.

Although the effect of various factors on adsorption hysteresis is not fully understood, the shapes of hysteresis loops have often been identified with specific pore structures. Hysteresis appearing in the multilayer range of physisorption isotherms is usually associated with capillary condensation in mesopore structures. Such hysteresis loops may exhibit a wide variety of shapes like Type IV and V. A feature common to many hysteresis loops is that the steep region of the desorption branch leading to the lower closure point occurs (for a given adsorptive at a given temperature) at a relative pressure which is almost independent of the nature of the porous adsorbent but depends mainly on the nature of the adsorptive (e.g. for nitrogen at its boiling point at p/p^o 0.42 and for benzene at 25°C at p/p^o 0.28).

In view of the complexity of real solid/gas interfaces and the different mechanisms which may contribute to physisorption, it is hardly surprising to find that none of the current theories of adsorption is capable of providing a mathematical description of an experimental isotherm over its entire range of relative pressure. As also highlighted by the research performed by Jurinak [40], Type III , IV, and V are uncommon, while Type I and II are common. In comparing the five isotherm types shown in (Fig.5.1), the Type I isotherm yields the most favourable characteristic (maximum water uptake at lower relative pressure range) [40]. The choice of desiccant is one of the key elements in the energy wheel technology. Silica gel and molecular sieves are the desiccants currently being most widely used for the enthalpy wheels.

The general sorption curve (Equ. 5.1.1) presented in [40] is now widely used to model the sorption characteristics of the most available desiccants in the market such as silica gel and molecular sieves. The desiccant isotherm shape describes how a desiccant material adsorbs moisture at different levels of relative humidity (Φ).

$$\varphi_{ms} = \frac{\varphi_m}{\varphi_M} = \frac{\Phi}{S + (1 - S)\Phi} \tag{5.1.1}$$

where:

- φ_{ms} is the specific moisture content in the desiccant $[-]$;
- φ_M the maximum moisture capacity loadind of desiccant at 100% relative humidity $[\frac{kg_v}{kg_d}]$;
- φ_m is the moisture content in the desiccant $[\frac{kg_v}{kg_d}]$;
- S is the separation factor that defines the isotherm shape $[-]$;
- Φ is the relative humidity in the fluid [%];

For different values of φ_M and S , different types of desiccant isotherm shapes can be produced (5.2).

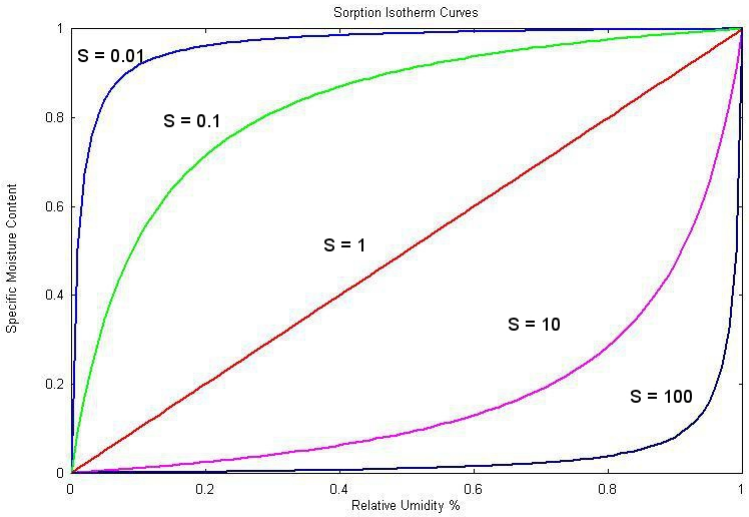

Figure 5.2: The sorption isotherm curves changing the S parameter

In practice, the Jurinaks adsorption isotherm model is widely used to model the desiccant matrix. The model was developed based on the Clausius-Clapeyron equation. The concept of the model rises from the differences between the thermodynamic characteristics of adsorbed water vapor by the desiccant matrix and the condensed water vapor on the surface of the matrix. Therefore, the heat of sorption, heat released when the air changes from a gaseous phase to an adsorbed phase, is different than the heat of vaporization, heat resealed when air changes from gaseous a phase to a condensed layer of bulk water phase.

The heat of soiption and the heat of vaporization can be defined, using the Clausius − Clapeyron equation, as

$$h_{ad} = RT^2 \frac{\partial ln P_v}{\partial T} \tag{5.1.2}$$

$$h_{vap} = RT^2 \frac{\partial ln P_{vsat}}{\partial T} \tag{5.1.3}$$

where:

- h_{ad} is the differential heat of adsorption $[\frac{KJ}{kg}]$;
- h_{vap} is the specific heat of vaporization $[\frac{KJ}{kg}]$;
- R is the gas constant for water $[\frac{KJ}{kgK}]$;
- T is the thermodynamic temperature $[K]$;
- P_v is the partial pressure of water vapor in the air $[Pa]$;
- P_{vsat} is the partial pressure of water vapor at saturation $[Pa]$.

The change from water vapor to adsorbed phase can occur in unsaturated or saturated air, while the vaporization/condensation occurs only if the air is saturated as can be seen from equations (5.1.2) and (5.1.3) respectively. The energy effects of the two phenomena can be related as:

$$\Big(\frac{\partial ln P_v}{\partial P_{vsat}}\Big) = \frac{h_{ad}}{h_{vap}} = h^* \tag{5.1.4}$$

Jurinak [[40]] assumed that hi is independent of temperature and can be only a function of matrix water content. Based on this, he derived the following empirical correlation which can be used to reproduce all isotherm types:

$$\frac{h_{ad}}{h_{vap}} = h^*(\varphi_m) = 1 + \Delta h^* \frac{e^{K\varphi_{ms}} - e^K}{1 - e^K}. \tag{5.1.5}$$

The constants Δh^* and K are used to determine the isotherm shapes: $1 + \Delta h^*$ is h^* at φ_{ms} equal to 0.

To find relative humidity Φ, equation (5.1.5) can be integrated to show that if the adsorption isothenn is a function Glam) at temperature T_o , then at any temperature T_m the relative humidity of moist air in equilibrium with the desiccant is

$$\Phi = G(\varphi_m)\Big(\frac{P_{vsat}(T_m)}{P_{vsat}(T_o)}\Big)^{h^*-1}. \tag{5.1.6}$$

The form of equation (5.1.5) used insures that isotherms given by equation (5.1.6) converge to the maximum water content φ_M at $\Phi = 1$. This allow φ_M to be used as a scaling parameter for the isotherms. The physical assumption implicit in this behavior of isotherms is that at saturation (φ_M), adsorption becomes normal condensation on

the matrix.

To find the function $G(\varphi_m)$ the general isotherm relation is used (5.1.1 and the relative humidity in equilibrium with a desiccant surface can be expressed as

$$\Phi = \frac{S\varphi_{ms}}{1+(S-1)\varphi_{ms}}\left(\frac{P_{vsat}(T_m)}{P_{vsat}(T_o)}\right)^{h^*-1} = \frac{S\varphi_m}{\varphi_M+(S-1)\varphi_m}\left(\frac{P_{vsat}(T_m)}{P_{vsat}(T_o)}\right)^{h^*-1}. \quad (5.1.7)$$

The local equilibrium (isotherm) relation is an empirical relation, different for each desiccant.

5.1.1 Desiccant characterization

The transport phenomena inside the porous desiccant medium are governed by the conservation equations for the mass of vapor and of adsorbed water and the thermal energy. The locally thermodynamic equilibrium in the mass conservation equations is imposed specifying the φ_{ms} based on the relation plotted in Fig.5.3 ([29])and in Fig.5.4 ([24]) for the different desiccant.

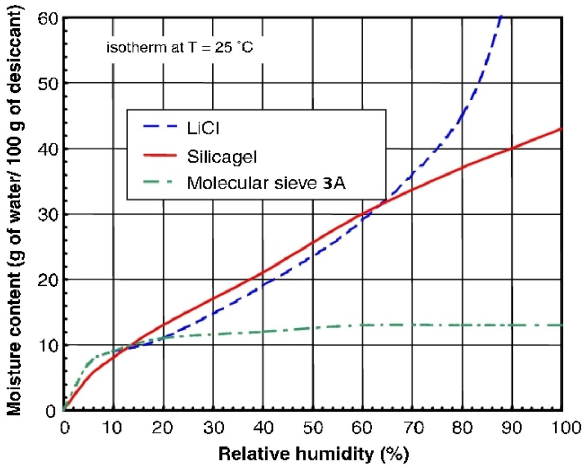

Figure 5.3: Comparison of Water vapor adsorption isotherms for silica gel - LiCl - Molecular Sieve at 25 °C

How well an enthalpy wheel performs is strongly dependent upon the desiccant chosen. Silica gel is one of the most commonly used desiccants. Il can absorb water up to 40% of its own wight and withstand relatively high acidic environments. Because of good water vapor adsorption characteristic, or sorption isotherm, over a wide range of relative humidity, silica gel has generally been the first-choice. In addition, it has no known toxic properties. However, the decrease in adsorption capacity of silica gel with increasing temperature is significant compared to a molecular sieve. Moreover, strong alkalis (e.g.

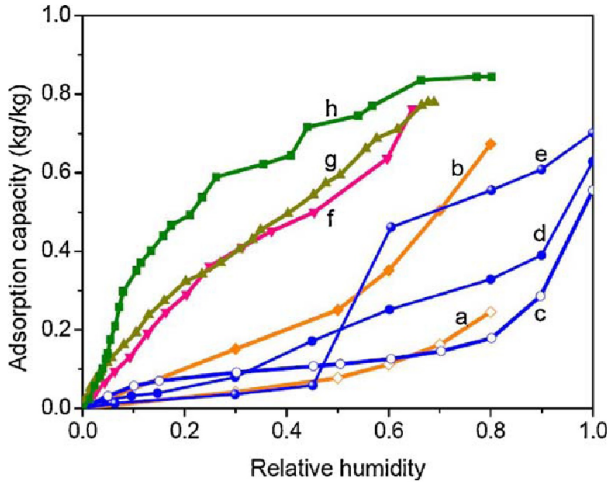

Figure 5.4: Water vapor adsorption isotherms for: (a) silica gel at 25 °C; (b) silica gel-$LiCl$ at 25°C; (c) sepiolite at 23°C; (d) sepiolite-carbon by chemical activation with steam at 23°C; (e) sepiolite-carbon by chemical activation with KOH at 23°C;(f) $CaCl_2 - SiO_2$ sol-gel at 25°C; (g) $CaCl_2 - MCM - 41$ at 20°C; (h) silica gel-$LiBr$ at 20°C

ammonia) may harm the silica gel.
Molecular sieves have a high sorption capacity at low water vapor concentrations, and maintain the high sorption capacity at elevated relative humidity. Its equilibrium water capacity is up to 20% by weight. Molecular sieves have no known toxic properties, but exposure to air that contains high concentrations of strong acids may harm them. The decrease in adsorption capacity of molecular sieve with increasing of temperature is much smaller than that of silica gel. On the other hand, the selective adsorption characteristic of molecular sieves can mitigate the indirect cross contamination problem. The 3Åmolecular sieves can provide excellent selective adsorption characteristic to water vapor (2,8Å) by excluding the adsorption of contaminant molecules that have a diameter grater than 3Å. Other desiccants, such as silica gel, oxidized aluminium and 4Åmolecular sieves do not provide the selective adsorption characteristic for water vapor.

5.2 State of the art for the production of hygroscopic materials

In common industrial practice with rotary exchangers are commonly used silica gels, aluminium oxides appropriately activated, natural and artificial zeolites, silicates, different types of synthetic polymers and with hygroscopic properties of inorganic salts such as calcium chloride, lithium chloride and lithium bromide . Among the various solutions studied in the field has attracted global attention the work proposed in [41]. In these

studies have been widely used new materials called Selective Water Sorbent (SWS), layers of conversion to be applied on systems very similar to those produced in this research. The conversion layer comprises a matrix meso-or micro-porous, more frequently based on silicates, then filled with the hygroscopic properties of inorganic salts. Other studies on these materials ([42]) indicate that it is possible to set the capacity of the sorbent layer varying the size of the porous matrix and the concentration of the hygroscopic salt to be included in the pores. The application of the hygroscopic layer can be made through the processes of immersion of the aluminium surfaces forming the rotor and is therefore easily accomplished in the industry. A further possibility for building materials with hygroscopic properties is to produce a growth of zeolites directly onto the surface of the desiccant wheel. Inspired by the work [43] you can produce the formation of zeolites using a first dive into appropriate solutions based on sodium silicates and hydrates of aluminium and a subsequent heat treatment. The up-take of water or other species in zeolites is called adsorption and functions on the basis of physisorption. The main driving force for adsorption is the highly polar surface within the pores. This unique characteristic distinguishes zeolites from other commercially available adsorbents, enabling an extremely high adsorption capacity for water and other polar components even at very low concentrations. In addition, the pore size plays a significant role, allowing or prohibiting the entrance of molecules to the pore system. The adsorption on molecular sieves is therefore dependent on the following physical molecular properties:

- Size and Shape: Molecules larger than the pore opening of the molecular sieve can not be adsorbed, smaller molecules can.

- Molecular Polarity: Molecules with large polarity or polarisability can be adsorbed preferentially under identical conditions

The adsorption process is fully reversible and of purely physical nature. The structure of the zeolite stays intact during the adsorption process (and its later regeneration), and dissolution effects like with other drying agents like calcium compounds can not happen.

5.3 Analysis of experimental production of hygroscopic coatings

In the course of this research, I was able to follow the analysis and the development and testing prototype of a hygroscopic material made by the Department of Chemical Science and Technology of University of Udine ([44]). This was a research program in collaboration with the company Geo.Coil srl. The main aim was to optimize the deposition process and coating performances in a typical aluminum foil for enthalpy wheels. It will also evaluate the possibility of incorporating zeolite structures of hygroscopic salts such as calcium chloride and lithium bromide in order to have a synergic effect between the two materials.

5.3.1 Coatings based on silicon alkoxides (TEOS)

The surface textures of a TEOS (tetra-ethyl-ortho-silicate, or equivalently tetra-ethoxy-silane) coated foil is shown in in Fig 5.5. Hygroscopic salts ($CaCl2$) are added to TEOS in order to provide hygroscopic properties. The main aim is to obtain a uniform, smooth, defect free layer. Here a good adesion was obtained. Unfortunately ,Fig 5.6 and 5.7, where there are presented two spectrum analysis of coating materials in different points, highlight several imperfections of characteristic: crater-like, non-uniform deposition. Such imperfection might be removed via an optimisation oftimes and temperature parameters of coated production.

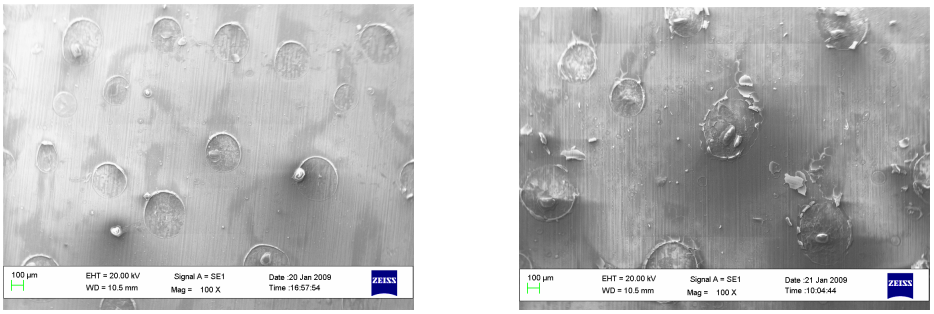

Figure 5.5: TEOS coatings S and SFC

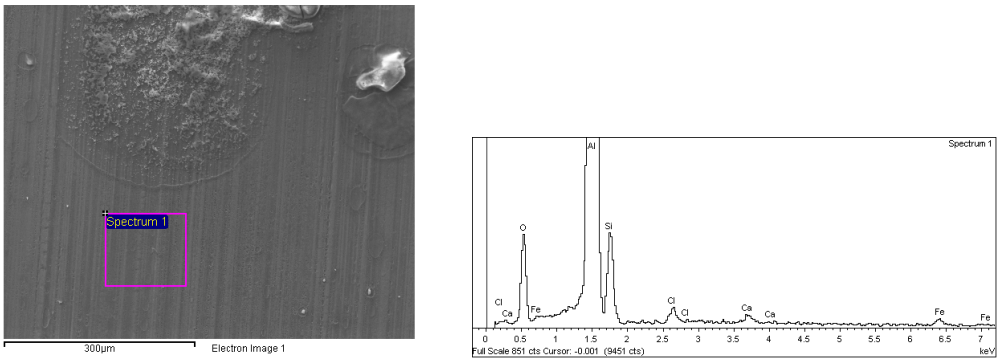

Figure 5.6: TEOS spectrum analysis 1

5.3.2 Coatings based on Zeolite

Zeolite molecular sieves are crystalline, highly porous materials, which belong to the class of alumino silicates. These crystals are characterised by a three-dimensional pore system, with pores of precisely defined diameter. This diameter is in the dimension of

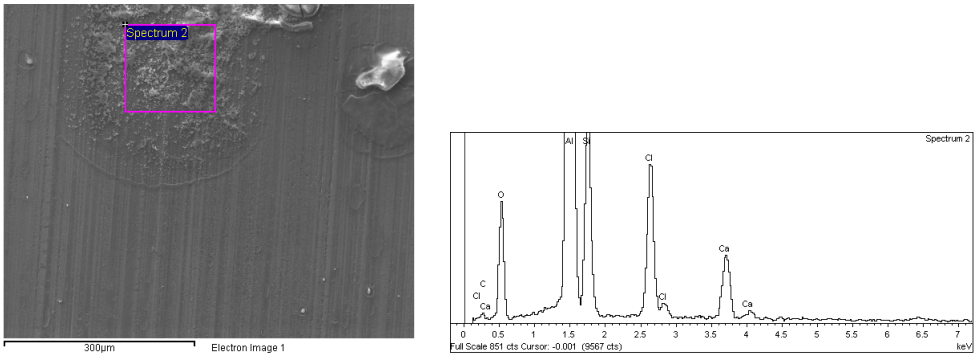

Figure 5.7: TEOS spectrum analysis 2

the size of molecules such as water, CO_2 and H_2S. The pores can be adjusted to precisely determined uniform openings allowing for molecules smaller than its pore diameter to be adsorbed whilst excluding larger molecules, hence the name molecular sieve. The different pore sizes of synthetic zeolites open up a wide range of possibilities in terms of "sieving" molecules of different size or shape from gases and liquids.

Molecular sieves are manufactured by crystallisation from aluminium hydroxide, sodium hydroxide and waterglass. Under carefully controlled conditions, the crystallisation process produces the required sodium alumino silicate structure. The zeolite crystals can then be ion exchanged to adjust the pore size. After drying the molecular sieve crystals can either be processed to activated zeolite powder, or a small quantity of binder is added, forming the material into beads. These beads are dried, calcined and finally screened to the required particle size prior to packaging.

The final resul is shown in Fig 5.8. Again the surface is fully covered by coating; nonetheless, we still have the presence of non uniformities and defects. These assume different shapes, with respect to the previous TEOS case, due to the different manufacturing precess.

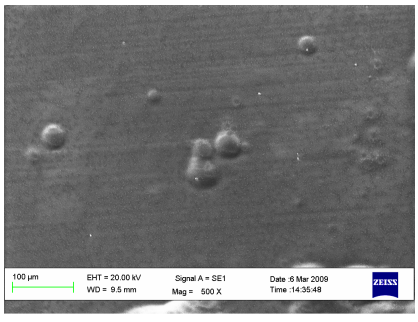

Figure 5.8: Zeolite based coating

5.3.3 Coatings based on Sodium silicate

The properties of silica gels are a result of the size and state of aggregation of the primary particles and their surface chemistry. Modern silica gel technology enables the production of highly pure gels that are composed of nearly 100% SiO_2 with tailor-made pore systems and surface properties. Silica gels can be produced from different raw materials. However, the synthesis from mineral acids, e.g. sulfuric acid, and aqueous sodium silicate is the only industrial relevant process today. Sulfuric acid and sodium silicate are mixed under controlled conditions to build the primary particles of the desired size, which polymerize and form the raw gel from which all types of silica gels are made.
By controlling the washing, ageing, and drying conditions, the important physical parameters such as porosity, pore size, and surface area can be adjusted to produce a range of different silica gel types. Silica gels are available in a wide range of particle sizes, each type having a well-defined particle size distribution. The type of mill applied during the grinding step and the use of a classifier allow for the manufacturing of fine-sized products.

Analyses of samples from the first specimen coated with acidified solutions of silicates has demonstrated that it was possible to apply a thin layer of silica with a well, uniform surface. As an example, images obtained by scanning microscope (SEM) and chemical analysis conducted by EDAX surface of an aluminium foil coated with silica by immersion are given in Fig 5.9 with a solution of 1/3 by weight of sodium silicate and 2/3 of water acidified with nitric acid 2.5% by weight. Fig 5.9 shows that, even for this first not yet optimized attempt, on the surface we cannot notice any relevant imperfections. Furthermore EDAX samples on two different location confirm the uniform presence of sodium silicate of the coating layer.The absence of cracks and flaking also shows how this kind of coatings can adhere well to the substrate.

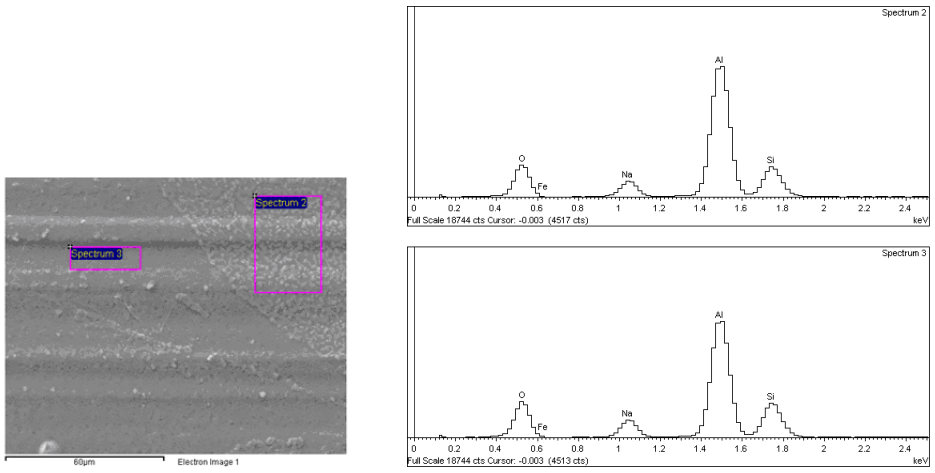

Figure 5.9: Sodium silicate based coating

5.4 Identification and development of silica-based baths

Following the analysis of the results on various types of hygroscopic material, it was decided to focus research towards the development and optimization of sodium silicate bath treatment. The following are the main results obtained.

5.4.1 Materials used

Given the potential of the system, it is preferred to use directly an industrial material purchased from commercial solutions Ingessil Ltd., precisely the SS2740 and SS2840, both with a rate of 26% SiO2 by weight, similar to that adopted for the silicate early production of coatings. The substrates are aluminium rotor blades supplied by Geo.Coil srl .

5.4.2 Production of the treatment solution

Different solutions were considered in order to find the best chemistry for the production of uniform films of silicates with high roughness. The procedure adopted for the production of all the baths is the following:

- Acidification of the water with a stated percentage of pure nitric acid at 98%.
- By keeping the solution under continuous agitation, the acidified water is added to sodium silicate.
- The solution is stirred continuously for at least an hour.

The baths were stored in polyethylene containers or in glass bottles. The composition of the solutions investigated is summarized in the table 5.1:

Label	Product	Silicate volume / volume solution	Wt% acid in the water
27 1/3 Si 1.0% H	2740	1/3	1.0
27 1/3 Si 2.5% H	2740	1/3	2.5
27 1/2 Si 1.0% H	2740	1/2	1.0
27 1/2 Si 2.5% H	2740	1/2	2.5
28 1/3 Si 1.0% H	2840	1/3	1.0
28 1/3 Si 2.5% H	2840	1/3	2.5
28 1/2 Si 1.0% H	2840	1/2	1.0
28 1/2 Si 2.5% H	2840	1/2	2.5

Table 5.1: Silicate solutions examined

5.4.3 Procedure for the production of coatings

The rotor aluminium sheets were washed in a bath containing surfactants (laboratory experience a mild degreaser was used at concentrations of 1 g / l of water) and subjected to ultrasound. The samples were then dried. This procedure is essential to clean and standardize the surface and thus obtain homogeneous adhesion of the coating based on silicates. Each sample was immersed and extracted from the solution at a constant speed equal to 1 cm / s. To avoid the drop formation, the foil,before total extraction, has been left partially submerged for 1 cm in order to allow excess solution to flow back into the baths. All samples were then left to dry for 5-10 minutes before being heat-treated for 4 minutes at 120 °C. Rotors, when placed in the oven, were placed on absorbent paper.

In order to verify the chemical stability of these coatings baths were obtained from the same solutions at different ageing times and then compared with each other.

5.4.4 Ageing Solutions

The solutions, which have been tested for weeks, by an optical examination appear to be stable. Neither precipitations, nor fogging, nor in the middle depositions was detected. We found only a slight decrease pH value, for all solution. This decreas, after a few weeks, is of the order of 1 tenth od unit. The solutions are still characterized by very alkaline values (11-12).

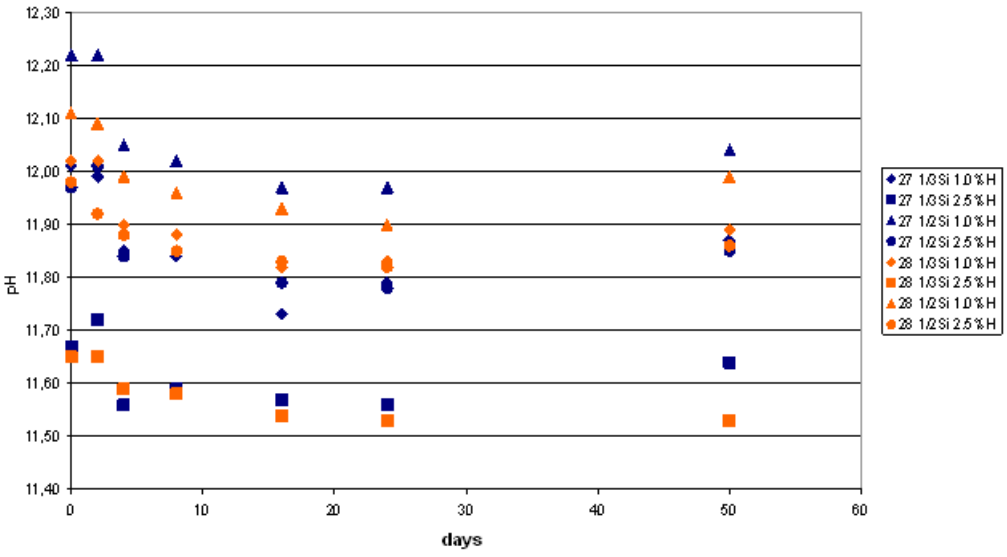

Figure 5.10: Ph - days ageing solutions

5.4.5 Evolution of micro−structure as a function of ageing solutions

In order to evaluate the influence of ageing of the solutions on the coating micro−structure we compare SEM images of rotor coated with different solutions based on Sodium silicate of different age. The substrates used are aluminium sheets of size 5 cm x 2.5 cm taken from the wheel material. The rate of extraction of silicates from the baths, for all of them, was of 1 cm / s. After waiting 5 minutes for partial drying, the samples were placed in a ventilated oven for another 5 minutes.

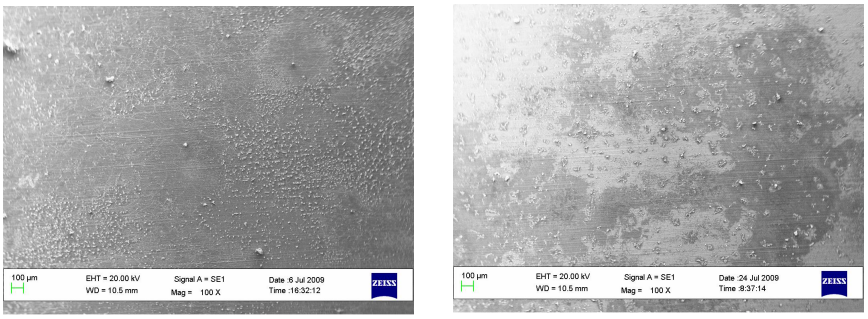

(a) `0days` (b) `24days`

Figure 5.11: Micro−structures solution 27 1/3 Si 1.0% H with ageing solutions

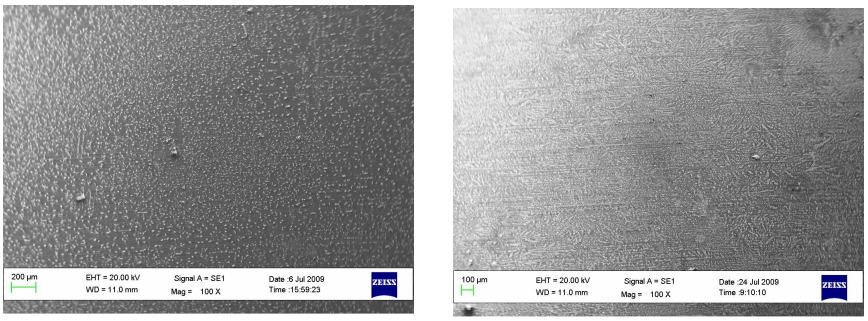

(a) `0days` (b) `24days`

Figure 5.12: Micro−structures solution 27 1/3 Si 2.5% H with ageing solutions

From the micro−graphs shown in Fig 5.11 to 5.18, the ageing of the solutions has an effect on the morphology of the coating. The ability of the film to adhere uniformly to the substrate appears, for all samples, good. The general impression is that the solution, ageing, results in coatings with micro−structures rougher and therefore more interesting.

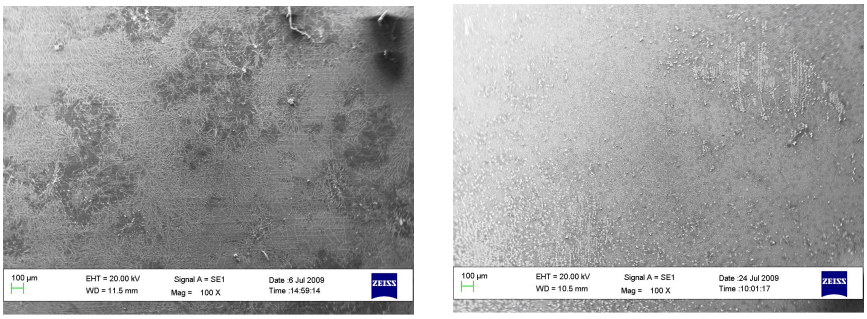

(a) `0days` (b) `24days`

Figure 5.13: Micro−structures solution 27 1/2 Si 1.0% H with ageing solutions

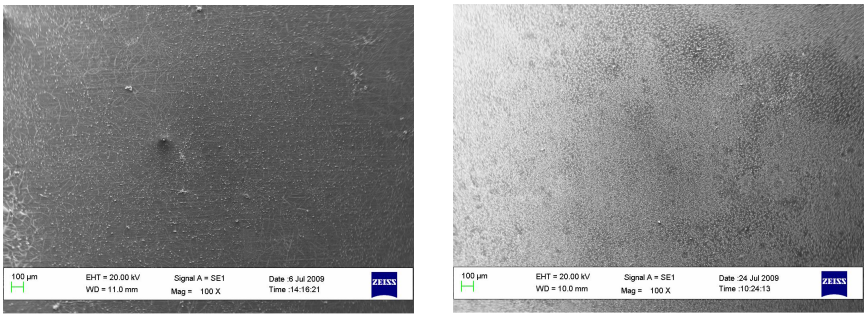

(a) `0days` (b) `24days`

Figure 5.14: Micro−structures solution 27 1/2 Si 2.5% H with ageing solutions

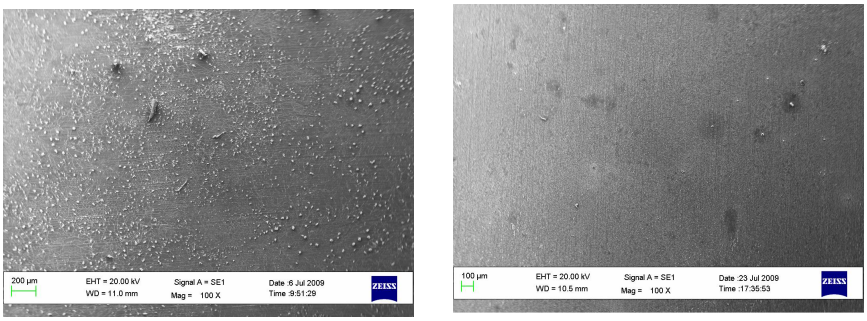

(a) `0days` (b) `24days`

Figure 5.15: Micro−structures solution 28 1/3 Si 1.0% H with ageing solutions

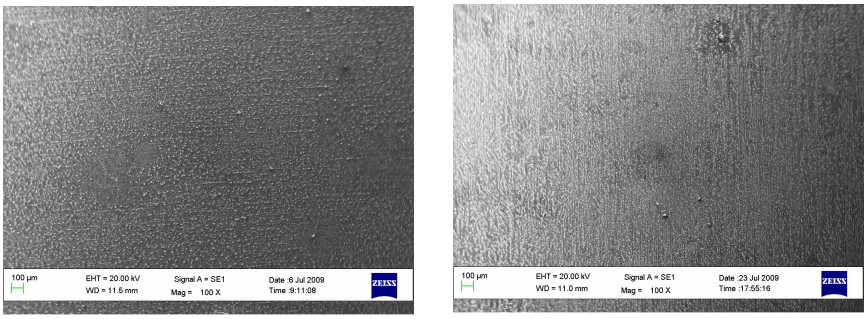

(a) `0days` (b) `24days`

Figure 5.16: Micro−structures solution 28 1/3 Si 2.5% H with ageing solutions

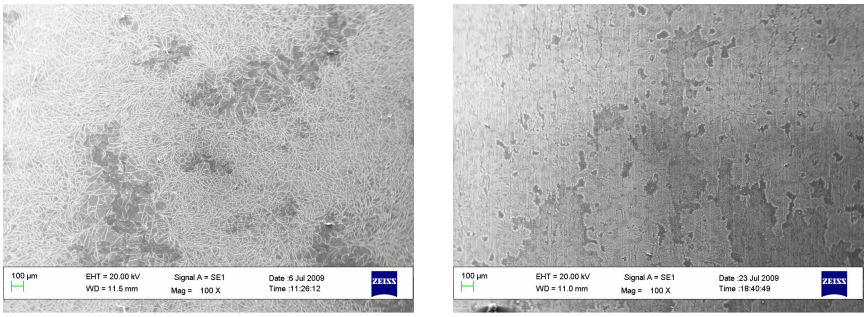

(a) `0days` (b) `24days`

Figure 5.17: Micro−structures solution 28 1/2 Si 1.0% H with ageing solutions

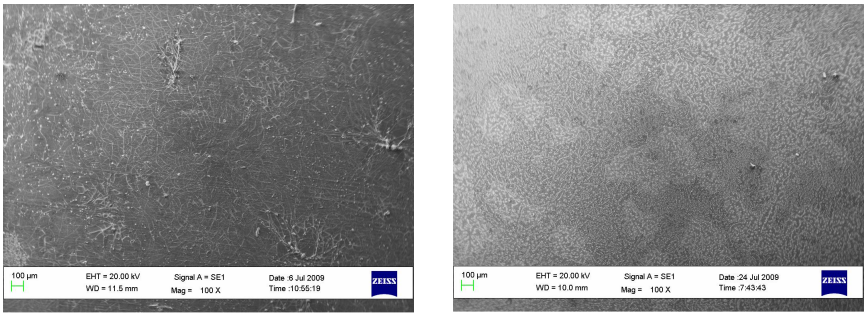

(a) `0days` (b) `24days`

Figure 5.18: Micro−structures solution 28 1/2 Si 2.5% H with ageing solutions

5.4.6 Quantification of the hygrocopical material deposited

A series od small scale rotors were prepared in order to evaluate the actual mass of hygroscopic material deposed with the coating. The analysis was performed weighting the dried rotors To quantify the hygroscopic material deposited small rotors have been prepared with the standard geometry and analysed before and after treatment. In general a cylinder of 6 cm in diameter and 20 cm in height was considered. In such case, 8-10 gramms of solution cover the rotor foils just after removal from bath. After 4 minutes thermal treatment at 100 °C 4 gramms are still on the foil surface. The missing material is assumed to be almost completely water. After 2 days the weight was further reduced, indicating that more water has left the system during drying. The new weight is 1 to 2 gramms more than the uncoated rotor. Knowing the density of the rotor based on the geometry of the wave (S/V), we can determine the amount of dessicant deposited per square meter. Dividing by the known density of dessicant is possible to estimate an average thickness of the layer. In the case under consideration we have obtained an average thickness of the hygroscopic coating of $0.01 - 0.05$ mm.

5.4.7 Coating stability under operating conditions

It is very important to ensure consistent performance for the wheel average operating life of the heat exchanger. Thus,to evaluate the effect of operating cycles on the stability of coated rotor . For this purpose, the following test was performed.
A rotor which has been applied silica-based coating has been subjected to a series of cycles characterized by the following steps:
Initial cycle (24h)

- from room temperature to 60°C / 100%RH humidity in about 1 hour;
- 60°C / 100%RH for 10 hours;
- Cooling from 60°C / 100% humidity at 5°C / 0% RH in 1 hour;
- 5°C / 0% for 1 hour;
- Cooling from 5°C / 0% humidity at −5°C / 0% RH in 1 hour;
- −5°C / 0% RH for 10 hours.

Cycle regime (24h)

- heating and humidification from −5°C / 0% RH to 60°C / 100%RH in about 1 hour;
- 60°C / 100%RH for 10 hours;
- Cooling from 60°C / 100% humidity at 5°C / 0% RH in 1 hour;
- 5°C / 0% for 1 hour;
- Cooling from 5°C / 0% humidity at −5°C / 0% RH in 1 hour;

- $-5°$C / 0% RH for 10 hours.

This test was performed to evaluate the possible loss in weight of the coating cycles during extreme hot/wet. Such loss would obviously result in degraded performance of the rotor. The data obtained are shown in the table 5.2:

Weight of the rotor All	116.9012 $[g]$
Weight of the rotor coated	
0 cycles	118.0102 $[g]$
4 cycles	119.5701 $[g]$
8 cycles	119.1265 $[g]$
12 cycles	118.3266 $[g]$
16 cycles	118.2420 $[g]$

Table 5.2: Weight of the rotor subjected to wet/dry cycles

In all the cases, we found an approximately equal weight, regardless the numbers of the number of cycles. The scattering of weights in table 5.2, which is not even monotone in time, is more likely due to experimental uncertainties rather than ageing effect. A possible cause of uncertainty is relevant to the weighting process which take place outside the climatic chamber and, thus, in not controlled conditions. It is therefore possible to say that the wet / dry cycles does not decomposed or remove the coating layer and the rotor to hold, depending on the situation in thermal environment, different percentages of moisture.

5.4.8 Analysis of two layers at different immersion time

In order to optimize the production process, we analyse the layer deposited via a two step immersion in the bath, as a function of the duration of the second immersion step. The first layer was obtained by immersion in solution at room temperature, heat−treated for 5 minutes at 100 °C. The second layer was still obtained by immersion, but always in a solution of silicate at 50 °C. Samplings were carried out at various intervals of time of immersion in the second solution.

Label	Immersion time second layer $[min]$
2X00	0
2X10	10
2X20	20
2X30	30

Table 5.3: Two layers with different time of immersion

The heat treatment is the same for all samples after all immersions: 5 min to 100 °C. These samplings were carried out to assess whether the time of immersion in the solution favoured the formation of layers at various morphologies.

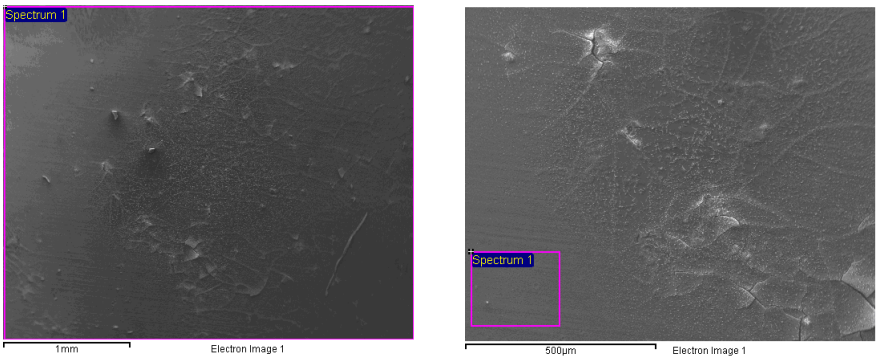

Figure 5.19: Micro−structures solution with two layers with 0 min of second immersion

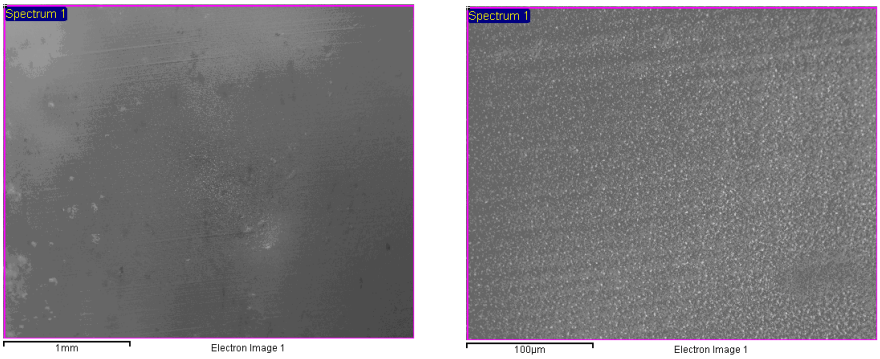

Figure 5.20: Micro−structures solution with two layers with 10 min of second immersion

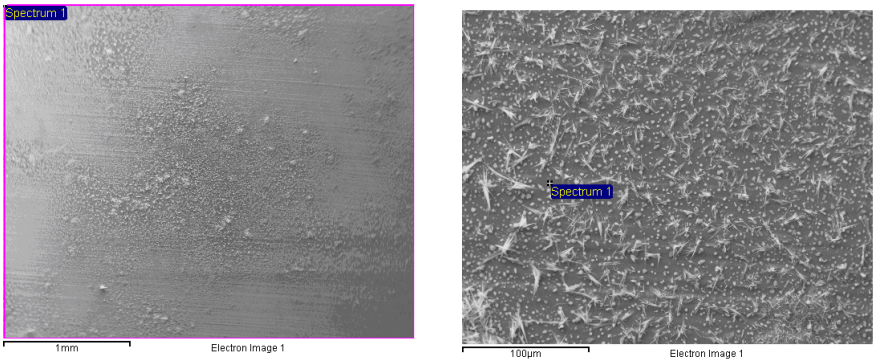

Figure 5.21: Micro−structures solution with two layers with 20 min of second immersion

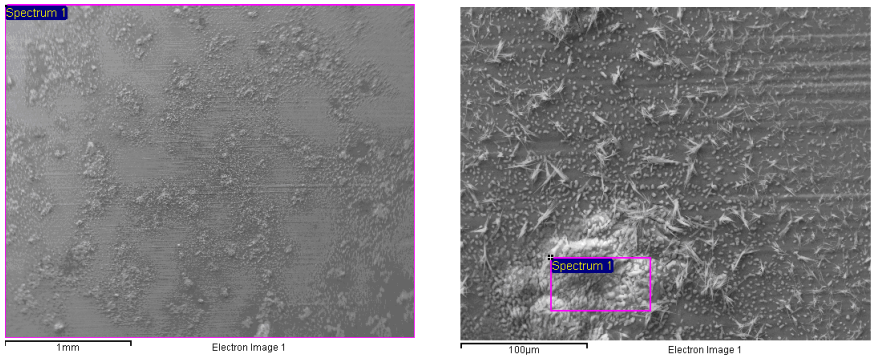

Figure 5.22: Micro−structures solution with two layers with 30 min of second immersion

From the Fig 5.19, 5.20, 5.21, 5.22 , you can see how, with increasing exposure time to the silicate solution, the film is morphologically more complex.The growth appears to occur through the formation of micro-needle, which tend to increase and interweave creating complex structures. The sample appears to be the best is the one marked by the initials 2X20, where the film height is nearly constant, but the surface appears to have a high degree of roughness due to a number of micropores, resulting in an increase in exchange surface without loss of properties of the coating. However, the coatings obtained with the double treatment do not justify the complication of the production.

5.5 Experimental enthalpy wheel

In parallel with the testing of small plates and rotors done at the University of Udine, the Geo.Coil research team has tried to replicate the same technology of the larger rotors (500mm Maximum diameter approx) to test both the technological feasibility and the results obtained in near real scale.

Figure 5.23: Experimental test equipment (source Geo.Coil srl)

Mixtures were used at different concentrations of silicates / nitric acid and various

dimensions of the rotors. With this method it is seen that in the process of drying the liquid film tends to thicken and therefore is not distributed evenly over the corrugated surface: in some tests a few channel might be fully blocked by the coating layer. This phenomenon must be avoided for the functionality of the exchanger. This happens because due to the increased processing time (due to higher thermal capacity and the lower heat transfer values) the coating liquid flows by gravity and accumulate at the rotor bottom. In order to limit this fact, it was decided to operate in the drying step with on horizontal continuosly rotating wheel. Furthermore, il was decided to to change the geometry of the corrugation of the two sheets of aluminium (bigger channels) with a modified roller.

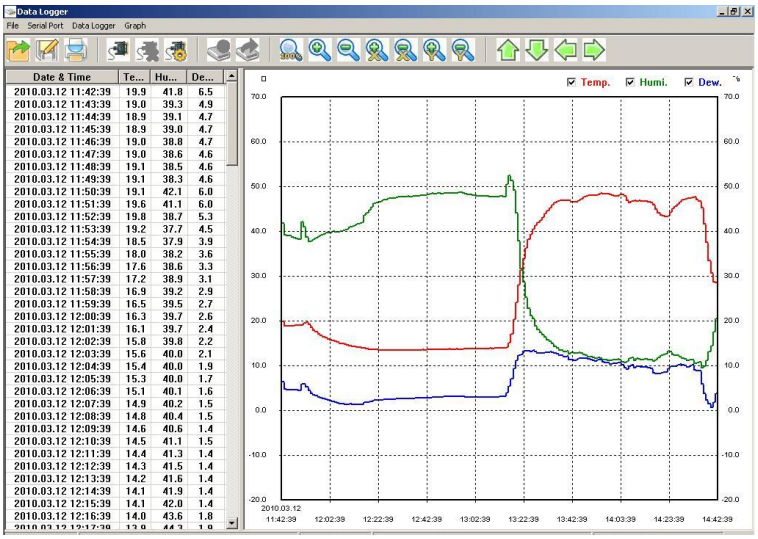

Figure 5.24: PCE data logger (source Geo.Coil srl)

The Geo.Coil team verificated and validated the results both from a thermodynamic and mechanically point of view. Since this test was to go hand in hand with the development of technology, it was decided to build an *ad hoc* full test ring for the recovery losses and thermodynamic efficiency evaluation (Fig 5.23). Although this equipment is not currently certified, it ended up being useful to provide a helpful indication of the performance of the regenerators. The experimental facility consist of a test channel, dual−circuit given PCE sensors temperature/humidity and pressure in order to make the necessary measurements (Fig 5.24). Once installed the 4 probes (two for each fluid before and after recovery) and tested the system, it was possible to prepare a campaign of measurements covering a wide range of operating parameters: namely wheel speed, input temperature and fluid mass flows. These measurements, in unsteady mode, could provide the necessary information on the thermodynamic performance of heat exchangers obtained with different hygroscopic materials (Tab. 5.4) and the dynamic response of such retrieval systems. These measurements were accompanied by fatigue tests to assess

Face velocity (m/s)	28 1/3 Si 1.0% H	28 1/3 Si 2.5% H	28 1/2 Si 2.5% H
winter conditions			
1.5	92.2	93.0	89.0
2.5	87.5	86.5	82.5
3.5	80.7	81.0	78.0
4.5	72.9	74.5	73.0
summer conditions			
1.5	90.6	92.0	93.2
2.5	81.8	86.0	87.5
3.5	79.5	80.0	76.3
4.5	73.6	74.0	75.4

Table 5.4: Total effectiveness for balanced flow in Geo.Coil test

their mechanical performance. The research team was able to determine the solution that meets the production requirements in terms of cost-effectiveness and logistics as well as the performance requirements, as weel as comparing the performances of various hygroscopic rotors obtained by varying the production parameters and those obtained with the commercial products.

5.6 Summary

Coatings containing silicates may produce several different layer morphologies. In light of the investigations conducted so far it seems that the solution that allows better deposition (dense and uniform roughness) is the 28 1/3Si 2.5% H which is composed with SS2840 Ingessi product, 1/3 silicate volume/silicate solution and 2.5 Wt % acid in the water: furthermore, it seems to be positively influenced by ageing, increasing pore roughtness and then, presumably, increasing the efficiency in moisture mass transfer due to the wide active area.

Of fundamental importance is that this experimental study as well as allowing an understanding of the various hygroscopic materials has provided the necessary information for the characterization of physical properties and dimensions of the hygroscopic layer used in the implementation of the enthalpy wheel model. As the competitive advantage in this business is mainly related to the hygroscopic coating used: the various manufacturers typically provide only qualitative information of the coating and hard quantitative.

6

Numerical model for enthalpy rotary exchangers

6.1 Mathematical model

The computational domain, as in the previous case, covers the whole wheel, as in Fig.2.3, z is oriented along the axes of rotation. Cartesian, rather than cylindrical, coordinates are used in order to allow for easy incorporation in a larger model including the whole recuperating system and the ducting, which usually is not axisymmetric.

6.1.1 Assumptions

The development of the mathematical model describing the heat and mass trasfer and fluid flow in the rotary regenerator is based on the following simplifying assumptions.

1. Eulerian approach in a non rotating frame of reference;
2. Constant mass flow rates,circumferential speed,inlet temperatures and water vapour density for both fluids;
3. No phase change occurs in the regenerator;
4. Incompressible flow of a constant properties flow with a negligible viscous dissipation;
5. Wall/fluid heat and mass transfer coefficient h, h_m independent of temperature and time and are constant along the air channels;
6. Rotating speed is slow enough to neglect wheel mechanical work production;
7. Heat transfer occurs only among the two fluids and the solid matrix;
8. The adsorption layer is thin enough to neglect any variation of mass transfer properties through its thickness. This allows to model it as a uniform porous material;
9. The hygroscopic capacity of matrix material is negligible;
10. The matrix dessicant material is always under equilibrium conditions .

6.1.2 Governing equations

The desiccant wheel model is based on the heat and mass balance in steady or unsteady state conditions. We do not model the individual channel geometries: the weel is assumed as as a porous material composed of a volume fraction of air within a metallic-hygroscopic material. The moist fluid is taken to be an ideal binary mixture of dry fluid and water vapour, characterized by conventional psychrometric relationships. Assuming an Eulerian point of view, the energy equations for the fluids became :

$$\rho_f c_f \phi \left(+ \frac{\partial T_f}{\partial t} + \mathbf{v_f} \cdot \nabla T_f \right) = k_f \phi \nabla^2 T_f + h \frac{A}{V} (T_m - T_f) \tag{6.1.1}$$

For a constant properties material, the energy equation for the solid matrix becomes :

$$\begin{aligned} \rho_f c_m (1-\phi) \left(+ \frac{\partial T_m}{\partial t} + \mathbf{v_m} \cdot \nabla T_m \right) &= k_m \left(1-\phi\right) \nabla^2 T_m \\ + h \frac{A}{V} (T_f - T_m) + \dot{m_v}''' (h_{ad} + c_{pv} (T_f - T_m)) & \end{aligned} \tag{6.1.2}$$

Mass balance of water vapour in the fluids:

$$\phi \left(+ \frac{\partial \varphi_f}{\partial t} + \mathbf{v_f} \cdot \nabla \varphi_f \right) = \phi D_f \nabla^2 \varphi_f - \dot{m_v}''' \tag{6.1.3}$$

Mass balance of water vapour in the desiccant:

$$(1-\phi) \left(+ \frac{\partial \varphi_d}{\partial t} + \mathbf{v_m} \cdot \nabla \varphi_d \right) = \dot{m_v}''' \tag{6.1.4}$$

where the moisture transfer is

$\dot{m_v}''' = \phi_d h_{mt} \frac{A}{V} (\varphi_m - \varphi_{mEq})$

and the moisture content in the desiccant in equilibrium is

$\varphi_{mEq} = \left(\frac{\Phi_f \varphi_M}{S + (1-S)\Phi_f} \right) / \rho_d .$

The relative humidity of the flow at the temperature T_f is:

$\Phi_f = \frac{\frac{\varphi_f}{\rho_f} P_{atm}}{(0{,}62198 + \frac{\varphi_f}{\rho_f}) P_{sat}(T_f)}$;

- ϕ is a porosity coefficient of the matrix;
- ϕ_d is a porosity coefficient of the desiccant
- $\mathbf{v_f}$, $\mathbf{v_m}$ are the actual fluid and matrix velocity fields inside each channel where the tangential velocities are imposed only by the wheel rotation;

- h_{mt} is the mass transfer coefficient;
- h_{ad} is the adsorption heat that was taken constant and the average value of $2700 kJ/kg H_2O$;
- φ_m is the mass fraction of vapour water in the desiccant;
- φ_M is the empirical coefficient used in the sorption isotherm describing the maximum moisture capacity of the desiccant (Es: Silica Gel $\varphi_M = 0,4$, Molecular sieve $\varphi_M = 0,2$)
- S is the separation factor that defines the shape of the sorption curve (Es: Silica Gel $S = 0.1$, Molecular sieve $S = 10$) .

The convective heat transfer coefficient h in Equ.(6.1.1) was obtained from numerical simulations of simultaneously (thermal and hydrodynamic) developing flow in a sinusoidal duct. Convective mass transfer coefficient($h_{mt}[m/s]$) was determined by using the analogy between heat and mass transfer. With the addition of the fundamental psychometric relationships for moist air, the formulation of the enthalpy wheel problem is fully closed.
The transport phenomena inside the porous desiccant medium are governed by the conservation equations for the mass of vapour and of adsorbed water and for thermal energy. Since the layer of the desiccant is assumed as an integral part of the porous medium, the moisture is evenly distribuited on the computational domain and we assume an instantaneus response, so that we always get equilibrium with the fluid.

The problem is well posed since the convection source term $h\frac{A}{V}(T_f - T_m) + \dot{m_v}'''(h_{ad} + c_{pv}(T_f - T_m))$ offers the required coupling and constraint on the solid matrix temperature and heat of phase change.

In the present model, the desiccant wheel operates at or near atmospheric pressure, where no condensation happens. If the desiccant wheel works under hight pressure, condensation might occur in the regeneration process. Sample models for desiccant wheels operating at high pressures are given ([45]).

Dessicant wheel

It is worth noting that the parameters of the proposed model can be set so as to describe the behaviour of desiccant wheel: changing the values of the parameters of the matrix (from aluminium to paper/plastic/glass), the speed of rotation and the type/amount of desiccant wheel can simulate a desiccant exchanger.

6.1.3 Boundary and Inlet conditions

The following steady state Boundary and Inlet conditions are imposed:

- Fixed inlet fluid temperature T_f^0, $T_m^0 = cost$;

- Fixed inlet water vapour density φ_f^0, $\varphi_m^0 = cost$;
- The lateral surface of the wheel is adiabatic $\frac{\partial T_f}{\partial n} \Big|_{r=D/2} = 0$, $\frac{\partial \varphi_f}{\partial n} \Big|_{r=D/2} = 0$;
- In the solid domain, all of the external surfaces are adiabatic $\frac{\partial T_m}{\partial n} \Big|_{r=D/2} = 0$, $\frac{\partial T_m}{\partial n} \Big|_{z=0,L} = 0$, $\frac{\partial \varphi_m}{\partial n}|_{r=D/2} = 0$, $\frac{\partial \varphi_m}{\partial n}|_{z=0,L} = 0$.

where D and L are respectively the diameter and the lenght in z-direction of the wheel.

6.2 Performance Parameters

If an averaged outlet bulk temperature at each wheel cross section is defined (for each fluid i, $i = h, c$) as in the following:

$$T_{bi} = \frac{\int_{S_{outlet}} v_i T_{fi} dS}{\int_{S_{outlet}} v_i dS} = \frac{1}{S_{outlet}} \int_{S_{outlet}} T_{fi} dS \tag{6.2.1}$$

we can obtain the sensible regenerator effectiveness from outlet bulk temperatures:

$$\epsilon_s = \frac{q}{q_{max}} = \frac{C_h(T_h^0 - T_{bh})}{C_{min}(T_h^0 - T_c^0)} = \frac{C_c(T_{bc} - T_c^0)}{C_{min}(T_h^0 - T_c^0)}. \tag{6.2.2}$$

The maximum reference heat flux q_{max} would be attained for a perfect a counter-flow recuperator of infinite surface area, zero longitudinal wall heat conduction and no leakages.

In the same way, averaged outlet water vapor

$$\varphi_{bi} = \frac{\int_{\varphi_{outlet}} v_i \varphi_{fi} dS}{\int_{S_{outlet}} v_i dS} = \frac{1}{S_{outlet}} \int_{S_{outlet}} \varphi_{fi} dS \tag{6.2.3}$$

and we can obtain the latent regenerator effectiveness from outlet water vapor:

$$\epsilon_l = \frac{W}{W_{max}} = \frac{C_h(\varphi_h^0 - \varphi_{bh})}{C_{min}(\varphi_h^0 - \varphi_c^0)} = \frac{C_c(\varphi_{bc} - \varphi_c^0)}{C_{min}(\varphi_h^0 - \varphi_c^0)}. \tag{6.2.4}$$

Once the entering and leaving air dry bulb temperature and humidity ratio conditions are known, the enthalpy values at each inlet and outlet state point can also be determined by the thermodynamic relations of moist air. Consequently, the total enthalpy effectiveness can be computed as:

$$\epsilon_t = \frac{Qt}{Qt_{max}} = \frac{C_h(h_h^0 - h_{bh})}{C_{min}(h_h^0 - h_c^0)} = \frac{C_c(h_{bc} - h_c^0)}{C_{min}(h_h^0 - h_c^0)}. \tag{6.2.5}$$

To reduce the complexity of the numerical model of coupled heat and mass transfer in enthalpy recuperators, Simonson and Bersand ([11] and [12]) proposed correlations (6.2.6, 6.2.7, 6.2.8) for the sensible, latent and total effectiveness of enthalpy wheel for balanced flow by correlating their numerical model simulation data. This correlations give good

result for silica gel enthalpy wheel and a molecular sieve enthalpy wheel, although the uncertainty of the result increases to about ± 5% for the molecular sieve enthalpy wheel.

$$\epsilon_s = \frac{NTU_o}{1+NTU_o}\left(1-\frac{1}{7.5C_r^*}\right) - H^*\left[\frac{0.26\left(\frac{C_r^*}{\varphi_M^2 C_{rm}^*}\right)^{0.28}}{7.2(C_r^*)^{1.53}+\frac{210}{(NTU_o)^{2.9}}-52}+\frac{0.31\eta}{(NTU_o)^{0.68}}\right] \tag{6.2.6}$$

$$\epsilon_l = \frac{NTU_o}{1+NTU_o}\left(1-\frac{1}{0.54(C_{rmt}^*)^{0.86}}\right)\left(1-\frac{1}{(NTU_o)^{0.51}(C_{rmt}^*)^{0.54}H^*}\right) \tag{6.2.7}$$

$$\epsilon_t = \frac{\epsilon_s+\epsilon_l H^*}{1+H^*} \tag{6.2.8}$$

where

- $NTU_o = \left[\frac{1}{C_{min}}\right]\left[\frac{(hA)_c(hA)_h}{(hA)_h+(hA)_c}\right]$ the global number of transfer unit;
- $C_r^* = \frac{C_r}{C_{min}} = \frac{M_w c_w}{(\dot{m}c_{pf})_{min}t_0}$ the overall matrix heat capacity ratio;
- $C_{rm}^* = \frac{M_d}{\dot{m}_{min}t_0}$ the overall matrix moisture capacity ratio;
- $C_{rmt}^* = (C_{rm}^*)^{0.58}(\varphi_M)^{0.33}\left(\frac{\partial\varphi_{ms}}{\partial\phi}|_{\phi_{ave}}\right)^{0.2}(C_r^*)^{1.13}\left[\frac{e^{\left(\frac{1482}{T_{ave}}\right)}}{47.9}-1.26(\phi_{ave})^{0.5}\right]^{4.66}$ the storage of moisture in the desiccant layer;
- $H^* = \frac{\Delta H_l}{\Delta H_s} = (\frac{\Delta H_s}{\Delta H_l})^{-1} - 1 = 2500\frac{\Delta\varphi_f}{\Delta T_f}$ operating condition factor that represents the ratio of latent to sensible enthalpy differences between the inlets of rotary wheel.

These correlations are the main contribution of Simonson and Bersant's work: they are simpler than numerical models, but have not been widely used because they are still complex and require information that is often difficult to obtain, such as detailed geometrical and material properties.

6.3 Numerical implementation

As the in previous sensible model, we used the software COMSOL Multiphysics 3.5 for the implementation of the FEM: we used the same mesh and method of solution. We considered the four equations of balance and the equation of equilibrium in the desiccant was inserted as a "global function" on the whole domain.
In Fig.6.1 we can see a screenshot of Comsol software post-processor in the case of enthalpy whell .

Description	Parameter	Range
Friction of the phase change energy that is delivered directly to the air	η	$0 \leq \eta \leq 0.1$
Operating condition factor	H^*	$-6 \leq H^* \leq +6$
Overall number of transfer units	NTU_o	$2 \leq NTU_o \leq 10$
Overall matrix heat capacity ratio	C_r^*	$3 \leq C_r^* \leq 10$
Ratio of overall matrix heat capacity ratio to overall matrix moisture capacity ratio	$\frac{C_r^*}{C_{rm}^*}$	$1 \leq \frac{C_r^*}{C_{rm}^*} \leq 5$
Maximum moisture capacity of desiccant	φ_M	$0.1 \leq \varphi_M \leq 0.5$
Shape of the sorption curve	S	$0.01 \leq S \leq 100$
Ratio of the minimum to maximum heat capacity heat capacity rate of the air streams	C^*	$C^* = 1$

Table 6.1: Range of parameters used in Simonson and Bersand's effectiveness correlations

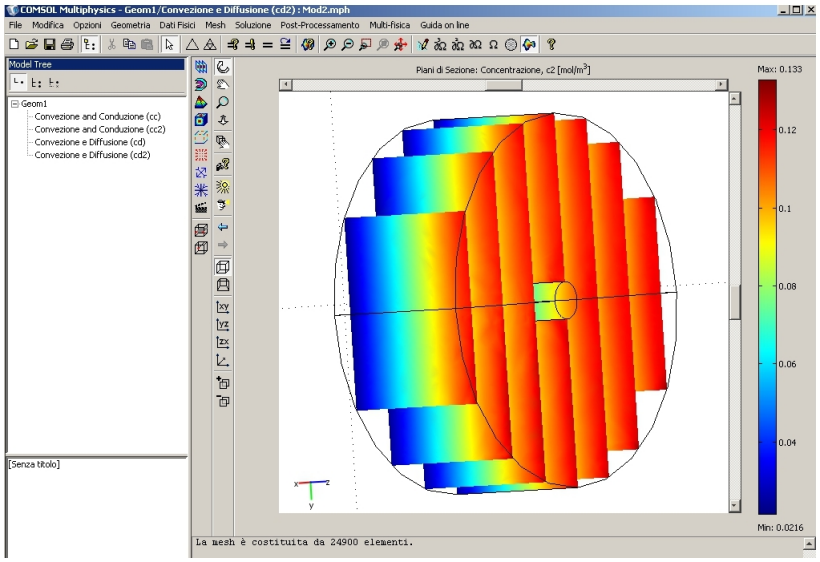

Figure 6.1: Screenshot of Comsol software enthalpy model

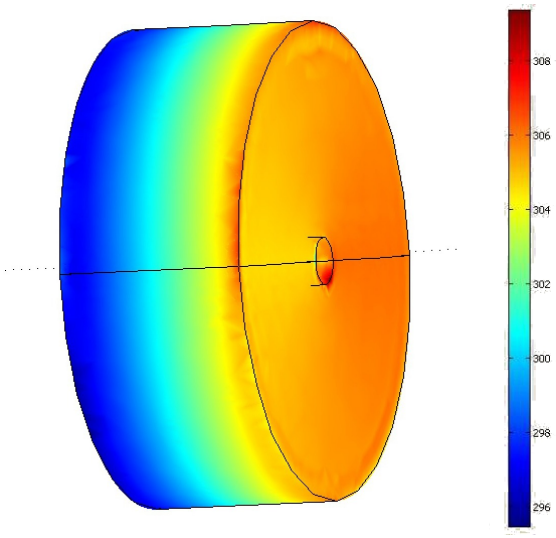

Figure 6.2: Temperature in the matrix - summer conditions

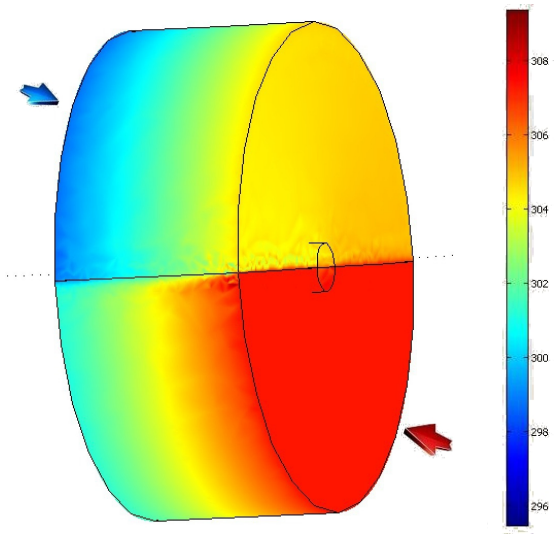

Figure 6.3: Temperature in the fluids - summer conditions

6.4 Thermal and Water vapor fields

With the proposed model, simply by using a commercial simulation software COMSOL, you can get in 3D all the information necessary to determine the heat and mass recovery. In Fig. 6.2, 6.3, 6.4,6.5 shows the temperature ranges and moisture density in reference

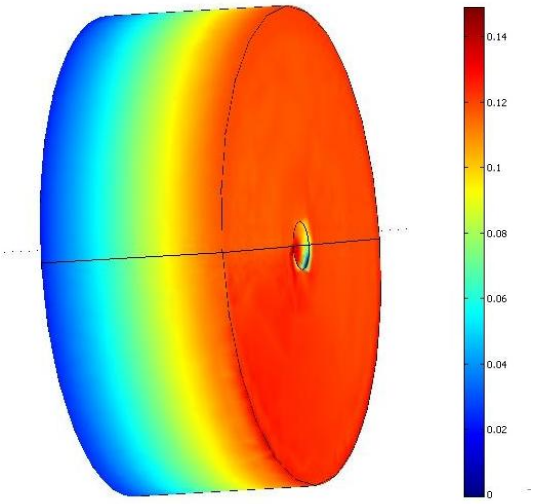

Figure 6.4: Water vapor density in the desiccant layer - summerconditions

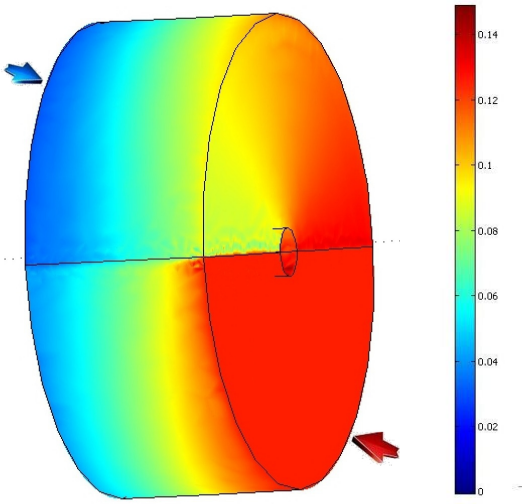

Figure 6.5: Water vapor density in the fluids - summer conditions

to the summer conditions in Table 6.2 for a enthalpy rotor with silica gel: the velocity of the fluid is equal to 4.5 [m/s] and the speed of rotations of 20 [PRM].

The high conductivity of the solid matrix yields the uniform solid temperature in the radial direction, Fig.6.2, while we get a clear stratification in the axial direction. This suggest a negligible influence of radial solid conductivity, a possible significant effect

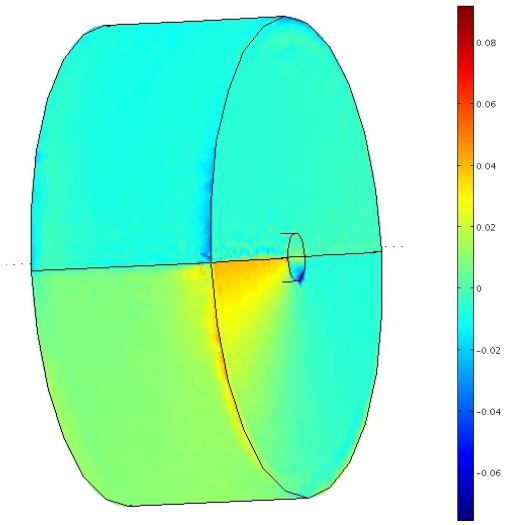

Figure 6.6: Rate of vapor change per volume in the desiccant layer- summer conditions

of axial solid conduction, and a negligible influence of the wheel diameter. Fig.6.3, as expected, shows a marked fluid temperature jump at junction between the hot and cold sectors.The exchange of mass affects the thermal field but this contribution (heat of evaporation - condensation) is lower than the convective exchange with the solid matrix. Similarly, the overlapping area of the vapor density in the fluid and the desiccant material could highlight the exchange of mass and the analogy between the exchange of heat and mass transfer.

6.5 Model validation

Condition	Item	Entering Outside Air (°C)	Entering Exhaust Air (°C)
Summer	DBT	35	24
	WBT	26	17
Winter	DBT	1.7	21
	WBT	0.6	14

Table 6.2: Standard rating condition (ANSI/ARI standard 1060-2001)

The model has been validated by comparison with both experimental data and manufactures' data on a large range of temperatures and humidity ratios (Table.6.2).

The total effectiveness comparisons for silica gel and molecular sieve enthalpy wheels under balanced flow conditions are presented in Fig. 6.8 and 6.7 at the summer and

	Silicagel	Molecular sieve
φ_M	0.4	0.15
S	0.1	10

Table 6.3: Parameters for local isotherm equilibriumin in the desiccant layer

Face velocity (m/s)	Proposed model	[11] and [12] correlation	Manufacturer's data
Silica gel			
1.5	93.2	93.0	92.0
2.5	87.2	87.0	86.0
3.5	80.7	81.5	80.0
4.5	74.5	76.5	74.0
Molecular sieve			
1.5	84.6	83.5	85.0
2.5	77.5	76.0	75.5
3.5	69.7	69.5	68.0
4.5	61.5	63.5	60.0

Table 6.4: Total effectiveness for balanced flow (summer rating condition)

Face velocity (m/s)	Proposed model	[11] and [12] correlation	Manufacturer's data
Silica gel			
1.5	93.5	93.2	93.0
2.5	88.7	87.4	86.5
3.5	83.5	82.0	81.0
4.5	77.8	77.0	74.5
Molecular sieve			
1.5	93.5	92.8	89.0
2.5	87.6	86.0	82.5
3.5	81.7	81.0	75.0
4.5	75.9	75.0	67.0

Table 6.5: Total effectiveness for balanced flow (winter rating condition)

winter Standard rating conditions, respectively. The rotational speed of the wheel is constant as 20 RPM. The face velocity of the fluids varies from 1.5 m/s to 4.5 m/s. As expected, the total effectiveness decreases with increasing face velocity.

The Figures 6.8 and 6.7 show that the model gives good results in all the studies cases. The deviation of the model compared to experimental and manufacturers' data is below the imposed tolerance except for few points. The results are better for silica

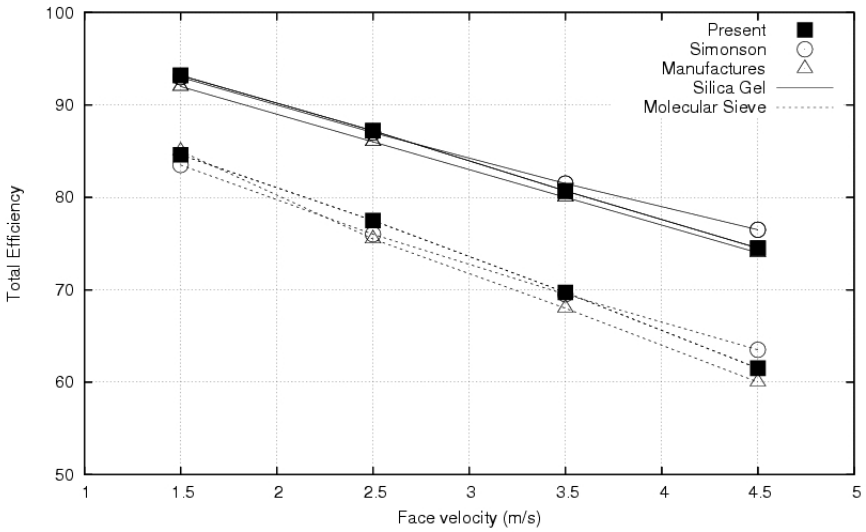

Figure 6.7: Total effectiveness comparison for balanced flow in summer rating condition

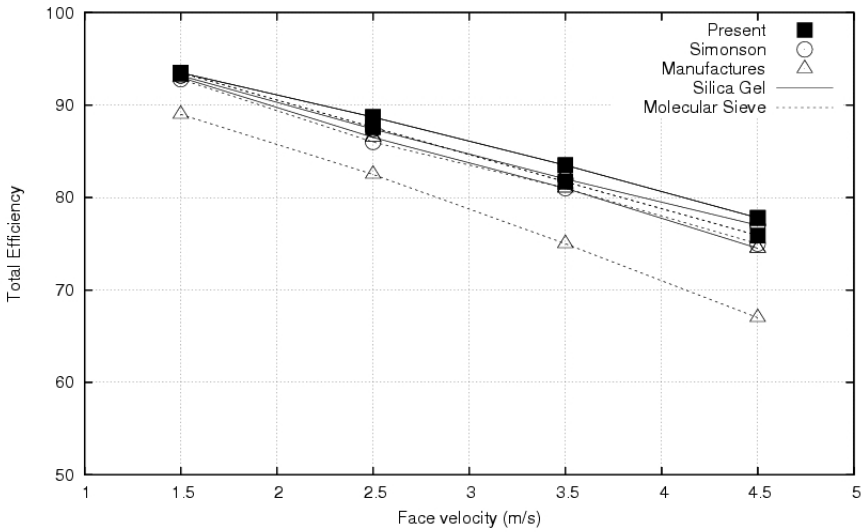

Figure 6.8: Total effectiveness comparison for balanced flow in winter rating condition

gel. The model was easily implemented in 3D using the commercial software COMSOL

Multiphysics 3.5. The simulations carried out with considerable our model showed that the overall efficiency of the heat exchanger depends on the characterization of the desiccant material and therefore only a careful analysis of all the operating conditions will determine the best choice.

6.6 Applications of the model

The proposed model is easily adaptable to various configuration of enthalpy rotary exchangers varying parameters in an appropriate way. As a sample tests, dynamic behavior and condensation case have been consided.

Dynamic behavior

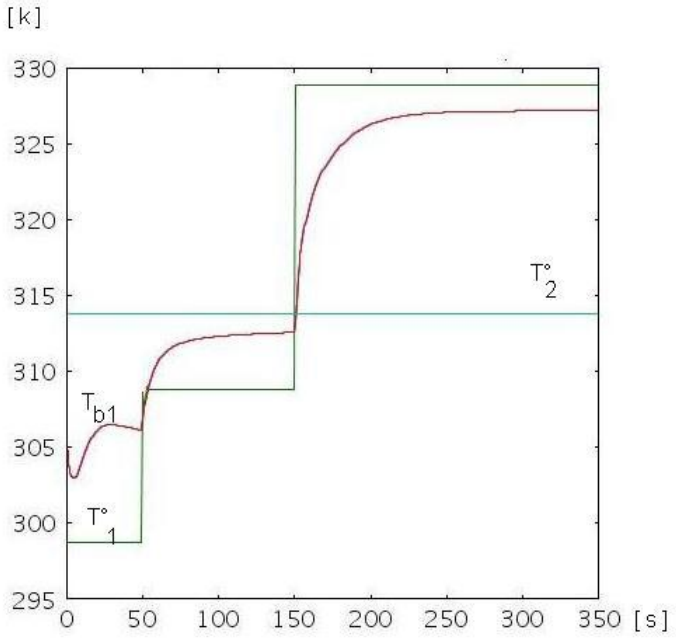

Figure 6.9: Time-dependent analysis

It is possible to consider unsteady inlet boundary conditions . To test the dynamic behavior for example, we analyzed the following case: temperature T_2 of exhaust air is constant while the temperature T_1 of outside air increases with two sharp step at $t = 50$ and $150[s]$. We monitor, as most significant parameter, the bulk temperature T_{b1}; neglecting the short transient at $t < 20[s]$ due to nonphysical initial conditions inside the rotor, T_{b1} stabilizes in a few minutes as shown in Fig.6.9, and then efficiency of the

exchanger remains constant.

In the field of application of the HVAC the time scale of the external temperature changes is of the order of a hour while reaction time for the rotary regenerators, as in Fig.6.9, are of the order of minutes: therefore it is reasonable to neglect the transient in such system.

Condensation

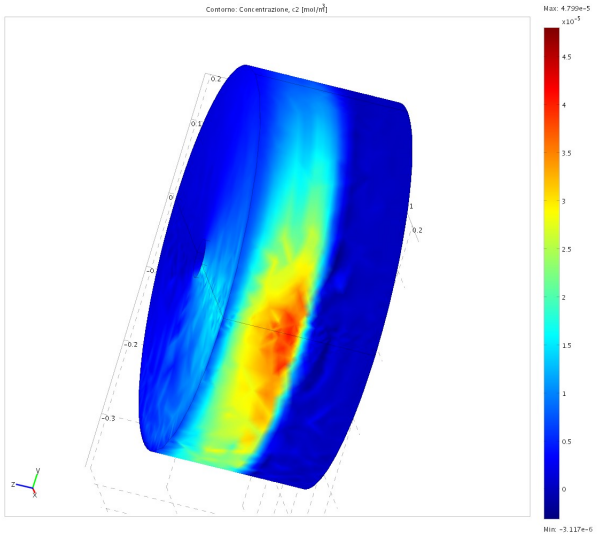

Figure 6.10: Density of condensed water

He was also analysed the case of condensation of water vapour contained in the fluid as the temperature of the matrix goes under the dew point temperature. Humification and dehumidification may occur also on uncoated aluminium wheels, if temperatures fall below dew point. In principle, it is possible to handle this conditions within the same numerical framework developed for enthalpy wheels. However, the mass transfer mechanism is highly non linear, and this may lead to convergence problems due to discontinuities generated by condensation. Some preliminary results are shown in Fig.6.10 where displays the concentration of water contained in the matrix neglecting neglecting the moviment of the water layer . At the present the results should be validated with experimental data and are therefore only qualitative.

6.7 Summary

Practical enthalpy wheel effectiveness model that can be more easily used to design and analyse enthalpy wheel integrated systems were develop from published complex formulations and models using statistical methods. The proposed practical model is for enthalpy wheel desiccant : silica gel or molecular sieve loaded onto an aluminium honeycomb matrix substrate. The model relate the sensible, latent and total effectiveness of the enthalpy wheel rotating integrating the values of variables in the output section of the fluid.

A general statement which adsorbent is better (silica gel or molecular sieve) is not possible. The greater efficiency depends on the operation conditions of the sorption wheel/unit, the quality of the coating and special characteristics of the adsorbent such as pore size, adsorption and regeneration behaviour. In dependency of temperature and humidity the absorption efficiency of water could be higher as well for silica gel as for molecular sieve.

This work was presented at the XXIX UIT Congress in 2011 ([46]).

Conclusions

In this analysis of the air−to−air rotary wheel, two models were developed: the sensible model and the enthalpy model.

A complete numerical model for sensible and enthaply rotary exchanger is developed to estimate the effectiveness of air−to− air energy wheel with or without a dessicant porous matrix and implemented in Comsol Software .

The model is intrinsically three-dimensional and transient with space (x, y, z) and time (t) as the independent variables.

Despite its simplicity, this model allows:

- great flexibility in the range of geometrical data;
- support for simulations the behavior with unbalanced flow / purge sector / different sectors for the flow;
- complete possibility in the particular characterization of the material dessicant.

Sensible model

In particular, the sensible model results show that:

1. during summer and winter operations, the sensible wheel can achieve the same effectiveness;
2. there is a good agreement between the numerical results and $\epsilon - NTU_o$ / Kays and London analytical solution;
3. set the geometry of the rotary exchanger, the possible combinations of operating parameters lies on the straight line in the plane $C_r^* - NTU_o$;

Enthalpy model

The main enthalpy model results are:

1. the enthalpy model predictions are found to be consistent with the results of Simonson and the "experimental" results;
2. using the enthalpy wheel instead of the sensible wheel in HVAC application is more realistic when the heat and moisture recovery are required;

3. in HVAC systems the enthalpy wheel provides enhanced performance in the sense that the wheel outlet conditions get more closer the desired indoor conditions (temperatures and humidity ratios) ;

4. The wheel efficiency strongly depends on the operating conditions;

An important contribution of this work is the modelling of the thermal wheel as a uniform porous media, where matrix/fluid shares the same computational domain. The details of single channel are no longer required but incorporated in the model parameters.Furthermore, the choice of a reference system Eulerian has made the boundary conditions more intuitive and therefore simple.

The main conclusion of this work is the identification of a model of rotary exchangers that is suitable for easy prediction of the dynamic behaviour of a sensible / enthalpy wheel.

The development of such model based directly on the manufacturer data of geometry of the wheel would be of great practical interest, and highly helpful to perform quick energy dynamic simulations of $HVAC\&R$ systems integrating enthalpy wheels, thus promoting the use of more efficient systems that allow the incorporation of renewable energy or waste energy recovery and furthermore the reduction of CO_2-emissions.

Future work

During this research, the focus was limited to estimate the effectiveness of a symmetric − balanced air−to−air energy wheel (or unbalanced but without considering the leakage of fluid between the two courses) with a porous matrix as heat and mass exchange media. Two theoretical and numerical models were developed to achieve these objectives. Many considerations were covered in this research; however, there are still some other issues that need to be investigated. Recommended future studies are as follows:

1. Experimental investigations of adsorption isotherm for the matrix material with wider range of operating conditions in this research are needed in order to derive the appropriate empirical coefficients ;

2. Numerical and experimental investigations of frost growth (or icing) within energy wheels are still needed. Frost control strategies can be also investigated

Definitions,Acronyms,Abbreviations

A	Solid matrix heat transfer surface	$[m^2]$
c	specific heat	$[J/kgK]$
C	Heat capacity	$[W/K]$
C^*	heat capacity ratio C_{min}/C_{max}	[-]
C_r	matrix total heat capacity	$[W/K]$
C_r^*	matrix exchanger heat capacity ratio	[-]
D	regenerator diameter	$[m]$
$\dot{m_v}'''$	moisture trasfer	$[kg_v/m^3s]$
NTU	Number of transfer unities	[-]
NTU_o	Global number of transfer unities	[-]
L	regenerator lenght	$[m]$
k	thermal conductivity	$[W/mK]$
h	heat trasfer coefficient	$[W/m^2K]$
h_m	mass trasfer coefficient	$[kg/m^2s]$
M	mass	kg
n	unit vector normal to the boundary	[-]
P	Pressure	[Pa]
R	ratio between time of crossing the wheel lenght and the rotation period	[-]
RPM	Revolutions Per Minute	[-]
T	temperature	$[K]$
DWT	Dry−Bulb Temperature	$[°C]$
WBT	Wet−Bulb Temperature	$[°C]$
t_o	rotation speed	$[s]$
S	separation factor	[-]
S_f	fluid passages cross section	$[m^2]$
u, v	trasverse velocity componets	$[m/s]$
w	axial velocity component	$[m/s]$
V	volume	$[m^3]$
$\dot{V}$	volumetric flow	$[m^3/s]$
ω	angular speed	$[rad/s]$
ϑ	angle in the plane x, y	$[rad]$
φ	specific moisture content	$[\frac{kg_v}{m^3}]$
φ_M	maximum moisture capacity of the desiccant	$[\frac{kg_v}{kg_d}]$
φ_m	moisture content of the desiccant	$[\frac{kg_v}{kg_d}]$
φ_{mEq}	specific moisture content of the desiccant at equilibrium	$[\frac{kg_v}{m^3}]$
ρ	density	$[kg/m^3]$
ϕ	porosity of matrix	[-]
ϕ_d	porosity of dessicant	[-]
Φ	relative humidity in the air	[%]

Subscripts and Superscrips

ave	average between the supply and exhaust inlet conditions
atm	atmospheric
c	cold stream
d	desiccant
f	fluid
h	hot stream
i	hot or cold stream
m	solid matrix
max	maximum between cold or hot streams values
min	minumum between cold or hot streams values
sat	saturation
tot	total

Bibliography

[1] Refrigerating American Society of Heating and Air-Conditioning. Standards for natural end mechanical ventilation. *ASHRAE*, Standard 62-73, 1977.

[2] Refrigerating American Society of Heating and Air-Conditioning. Ventilation for acceptable indoor air quality. *ASHRAE*, Standard 62-1981, 1981.

[3] Refrigerating American Society of Heating and Air-Conditioning. Ventilation for acceptable indoor air quality. *ASHRAE*, Standard 62-1989, 1989.

[4] Refrigerating American Society of Heating and Air-Conditioning. Ventilation requirement for acceptable indoor air quality. *ASHRAE*, Standard 62-2001, 2001.

[5] Refrigerating American Society of Heating and Air-Conditioning. Thermal environmental conditions for human occupancy. *ASHRAE*, Standard 55-1992, 1992.

[6] Refrigerating American Society of Heating and Air-Conditioning. Handbook of equipments. *ASHRAE*, 2001.

[7] C.Montery T.J.Lambertson. Performance factors of a periodic−flow heat exchanger. *Trans. ASME 15*, 80:586–592, 1958.

[8] A.L.London W.M.Kays. *Compact Heat Exhangers.* McGraw Hill, 1984.

[9] T.Skiepko R.K.Shah. Influence of leakage distribution on the thermal performance of a rotary regenerator. *Applied Thermal Engineering*, 19:685–705, 1999.

[10] R.K.Shah T. Skiepko. A comparison of rotary regenerator theory and experimental results for an air preheater for a thermal power plant. *Experimental Thermal and Fluid Science*, 28:257–264, 2004.

[11] R.W.Bersant C.J.Simonson. Energy wheel effectiveness: Part i−development and dimensionless groups. *International Journal of Heat and Mass Transfer*, 42:2161–2170, 1999.

[12] R.W.Bersant C.J.Simonson. Energy wheel effectiveness: Part ii− correlations. *International Journal of Heat and Mass Transfer*, 42:2171–2185, 1999.

[13] J.L.Niu L.Z.Zhang. Performance comparisons of desiccant wheels for air dehumidification and enthalpy recovery. *Applied Thermal Engineering*, 22:1347–1367, 2002.

[14] R.Z.Wang X.J.Zhang, Y.J.Dai. A simulation study of heat and mass trasfer in a honeycombed rotary dessiccant humidifier. *Applied Thermal Engineering*, 23:989–1003, 2003.

[15] F. Borup Z.Wu, R.V.N. Melnik. Model−based analysis and simulation of regenerative heat wheel. *Energy and Buildings*, 38:502–514, 2006.

[16] Matija Tuma B.Drobnić, Janez Oman. A numerical model for the analysis of heat transfer and leakages in rotary air preheater. *Int. J. of Heat and Mass Transfer*, 49:5001–5009, 2006.

[17] W.M. Worek L.A. Sphaier. Analysis of heat and mass transfer in porous sorbents used in rotary regenerators. *Int. J. Heat Mass Transfer*, 47:3415–3430, 2004.

[18] W.M.Worek L.A.Sphaier. Comparisons between 2−d and 1−d formulations of heat and mass transfer in rotary regenerations. *Numerical Heat Transfer, Part B:Fundamentals*, 49:3:223–237, 2006.

[19] Worek L.A.Sphaier, W.M. Parametric analysis of heat and mass transfer regenerators using a generalized effectiveness−ntu method. *Int.J.Heat Mass Trasfer*, 52:2265–2272, 2009.

[20] R.Z.Wang Y.J.Dai T.S.Ge, Y.Li. A review of the mathematical models for predicting rotary dessicant wheel. *Renewable and Sustainable Energy Reviews*, 12:1485–1528, 2008.

[21] A.R.Figueiredo C.R.Ruivo, J.J.Costa. Numerical study of the cyclic behavior od a dessicant layer of a hygroscopic rotor. *Numerical Heat Transfer, Part A: applications*, 53:1037–1053, 2008.

[22] S.M. Yoon J.D.Chung, D.Y. Lee. Optimization of desiccant wheel speed and area ratio of regeneration to dehumidification as a function of regeneration temperature. *Solar Energy*, 83:625–635, 2009.

[23] N.C.L.Brum C.E.L. Nobrega. Modeling and simulation of heat and enthalpy recovery wheels. *Energy*, 34:2063–2068, 2009.

[24] Y. Li R.Z. Wang T.S. Ge D. La, Y.J. Dai. Technical development of rotary desiccant dehumidification and air conditioning: A review. *Renewable and Sustainable Energy Reviews*, 14:130–147, 2010.

[25] S.D.White M.Goldworthy R.Narayanan, W.Y.Saman. Comparative study of different desiccant wheel designs. *Applied Thermal Engineering*, 31:1613–1620, 2011.

[26] P.J.Banks I.L.MacIaine-Cross. Coupled heat and mass trasfer in regenerators-prediction using an analogy with heat trasfer. *Int.J.Heat Mass Trasfer*, 15:1225–1242, 1972.

[27] T. Yilmaz O.Büyükalaca. Influence of rotational speed on effectiveness of rotary-type heat exchanger. *Heat and Mass Transfer*, 38:441–447, 2002.

[28] M. Sadrameli N. Ghodsipour. Experimental and sensitivity analysis of rotary air preheater for the flue gas heat recovery. *Applied Thermal Engineering*, 23:571–580, 2003.

[29] D. Marchio P. Stabat. Heat and mass trasfer modeling in rotary desiccant dehumidifiers. *Applied Energy*, 86:762–771, 2009.

[30] W.Aung S.Kaka¸c, R.K.Shah. *Handbook of single phase convective heat trasfer*. John Wiley & Sons - NY, 1987.

[31] L.Z.Zhang J.L. Niu. Heat transfer and friction coefficients in corrugated ducts confined by sinusoidal and arc curves. *Int. Journal of Heat and Mass Transfer*, 45:571–578, 2002.

[32] T.J.Lu D.T. Queheillat H.N.G. Wadley T.Wen, J.Tian. Forced convection in metallic honeycomb structures. *International Journal of Heat and Mass Transfer*, 49:3313–3324, 2006.

[33] L.Z.Zhang J.L. Niu. A numerical study of laminar forced convection in sinusoidal ducts with arc lower boundaries under uniform wall temperature. *Numerical Heat Transfer, part. A*, 40:55–72, 2002.

[34] H.Ghaebi S.Sanaye, S.Jafari. Optimum operational conditions of a rotary regenerator using genetic algorithm. *Energy and Buildings*, 40:1637–1642, 2008.

[35] M.R.Johnson G.P.Martin E.M.Sparrow, J.C.K. Tong. Heat and mass transfer characteristics of a rotating regenerative total energy wheel. *Int. J. Heat Mass Transfer*, 50:1631–1636, 2007.

[36] G.A.Longo R.Lazzarin. Innovazione tecnologica negli scambiatori rotativi. *Convenzione di ricerca fra Universitá degli Studi di Padova e la Geo.Coil srl*, 2003.

[37] G.Comini O.Pascoli, G.Croce. Numerical model for rotary exchangers recuperators. *Atti XXVII Congresso UIT sulla Trasmissione del Calore - Reggio Emilia 22−24 giugno 2008*, 1:257–262, 2008.

[38] R.A.W.Haul L.Moscou R.A. Pierotti J. Rouquerol T. Siemieniewska K.S.W.Sing, D.H.Everett. Reporting physisortion data for gas/solid systems. *Pure and Applied Chemistry*, 57:603–619, 1985.

[39] S.Brunauer. *The adsorption of gases and vapors*. Priceton University Press - NJ, 1945.

[40] W.M. Mitchell J.J. Jurinak. Effect of matrix properties on the performance of a counterflow rotary dehumidifier. *ASME Journal of Heat and Mass Trasfer*, 106:638–645, 1984.

[41] Y.J.Dai R.Z. Wang Z.J.Zhang, K.Sumathy. Dynamic hygroscopic effect of composite material used in desiccant rotary wheel. *Solar Energy*, 80:1058–1061, 2006.

[42] G.Cacciola V.N.Parmon Yu I. Aristov, G.Restuccia. A family of a new working materials for solid sorption air conditionin systems. *Applied Thermal Engineering*, 22:191–204, 2001.

[43] E. Proverbio G. Restuccia F. Russo L.Bonaccorsi, A. Freni. Zeolite coated copper foarms for heat pumping applications. *Microporous and Mesoporous Materials*, 91:7–14, 2006.

[44] L.Fedrizzi. Analisi e prototipazione di materiali igroscopici per recuperatori rotativi. *Convenzione di ricerca fra Universitá degli Studi di Udine − Dipartimento di Scienze e tecnologie Chimiche e la Geo.Coil srl*, 2010.

[45] W.M.Worker M.N.Golubovic. Influence of elevated pressure on sorption in dessicant wheels. *Numerical Heat Trasfer- Part A*, 45:9:869–887, 2004.

[46] G.Croce O.Pascoli. Numerical model for enthalpy rotary exchangers recuperators. *Atti XXIX Congresso UIT sulla Trasmissione del Calore - Torino 20− 22 giugno 2011*, page A7, 2011.